DR SHIGEYUKI TANAKA (Orcid ID : 0000-0002-3102-1440)

Article type : - Regular Manuscript

The functionally conserved effector Sta1 is a fungal cell wall protein required for virulence in *Ustilago maydis*.

Shigeyuki Tanaka*, Isabelle Gollin, Nicole Rössel and Regine Kahmann*

Department of Organismic Interactions, Max Planck Institute for Terrestrial Microbiology, Karl-von-Frisch-Straße 10, D-35043 Marburg, Germany.

*Correspondence to:
Dr. Shigeyuki Tanaka
Department of Organismic Interactions,
Max Planck Institute for Terrestrial Microbiology,
Karl-von-Frisch-Straße 10, D-35043 Marburg, Germany.
Tel. +49-6421-178-511
Fax +49-6421-178-599
Email : shigeyuki.tanaka@mpi-marburg.mpg.de

Prof. Dr. Regine Kahmann
Department of Organismic Interactions,
Max Planck Institute for Terrestrial Microbiology,

Karl-von-Frisch-Straße 10, D-35043 Marburg, Germany.
Tel. +49-6421-178-501
Fax +49-6421-178-509
Email : kahmann@mpi-marburg.mpg.de

Received: *12 November 2019*
Accepted: *18 February 2020*

ORCID
Dr. Shigeyuki Tanaka : https://orcid.org/0000-0002-3102-1440
Prof. Dr. Regine Kahmann : https://orcid.org/0000-0001-7779-7837

Summary

(1) The biotrophic fungus *Ustilago maydis* causes the smut disease of maize. The interaction with its host and induction of characteristic tumors are governed largely by secreted effectors whose function is mostly unknown. To identify effectors with a prominent role in virulence, we used RNA-seq and found that the gene *sta1* is upregulated during early stages of infection.

(2) We characterized Sta1 by comparative genomics, reverse genetics, protein localization, stress assays and microscopy.

(3) *sta1* mutants show a dramatic reduction of virulence and show altered colonization of tissue neighboring the vascular bundles. Functional orthologs of Sta1 are found in related smut pathogens infecting monocot and dicot plants. Sta1 is secreted by budding cells but is attached to the cell wall of filamentous hyphae. Upon constitutive expression of Sta1 fungal filaments become susceptible to Congo red, β-glucanase and chitinase, suggesting that Sta1 alters the structure of the fungal cell wall. Constitutive or delayed expression of *sta1* during plant colonization negatively impacts on virulence.

(4) Our results suggest that Sta1 is a novel kind of effector, which needs to modify the hyphal cell wall to allow hyphae to be accommodated in tissue next to the vascular bundles.

Keywords

Ustilago maydis, core effector, fungal cell wall, virulence, biotrophic pathogen

Introduction

Filamentous plant pathogens secrete effector proteins during host infection to suppress plant immunity and to modulate plant signaling and metabolism (Lo Presti *et al.*, 2015; Tanaka *et al.*, 2015b; Toruno *et al.*, 2016). Secreted effectors can either be delivered into the host cytoplasm to directly manipulate processes inside plant cells (cytoplasmic effectors), or can stay in the apoplastic space to protect fungal cells from plant defense components (apoplastic effectors). Apoplastic effectors required for virulence can be inhibitors of plant enzymes that can be detrimental to the pathogen like chitinases, peroxidase and proteases (Lange *et al.*, 1996; Tian *et al.*, 2004; Rooney *et al.*, 2005; Tian *et al.*, 2005; Tian *et al.*, 2007; van Esse *et al.*, 2008; Song *et al.*, 2009; Naumann *et al.*, 2011; Hemetsberger *et al.*, 2012; Mueller *et al.*, 2013; Okmen *et al.*, 2018). Apoplastic effectors can also attach to the fungal cell wall and the most prominent examples of these are LysM domain proteins, which bind chitin in the fungal cell wall and protect fungi from adverse effects of plant chitinases (de Jonge *et al.*, 2010; Marshall *et al.*, 2011; Mentlak *et al.*, 2012; Sanchez-Vallet *et al.*, 2013; Takahara *et al.*, 2016). Fungal cell wall bound effectors have also been shown to protect from antifungal host proteins (Ma *et al.*, 2018). These examples document that apoplastic effectors often play important roles in plant-pathogen interactions (Doehlemann & Hemetsberger, 2013; Wang & Wang, 2018).

Ustilago maydis is a biotrophic fungal pathogen causing smut disease in maize (*Zea mays*) (Banuett, 1995; Vollmeister *et al.*, 2012; Zuo *et al.*, 2019). Characteristic disease symptom elicited by *U. maydis* are tumors, which can develop on all above ground organs of the maize plant. *U. maydis* encodes several hundred putative secreted effector proteins and many of these contribute to virulence (Kamper *et al.*, 2006). A recent time-resolved RNA-seq analysis of *U. maydis* genes during host colonization revealed that the genes encoding putative secreted effector proteins are specifically upregulated and are expressed in waves during the course of fungal development on and inside the plant tissue (Lanver *et al.*, 2018).

Comparative genomics of smut pathogens uncovered that *U. maydis* and related smut fungi including the maize head smut pathogen *Sporisorium reilianum*, the sugar cane pathogen *Sporisorium scitamineum*, the barley pathogen *Ustilago hordei* and *Melanopsichium pennsylvanicum* infecting *Persicaria* species share a small number of core effectors (Schuster *et al.*, 2018). One of the

characterized core effector is Pep1, a protein of 178 amino acids containing four cysteine residues (Doehlemann *et al.*, 2009), which inhibits the activity of the apoplastic maize peroxidase POX12 (Hemetsberger *et al.*, 2012). The essential virulence-promoting function of Pep1 is conserved in other smuts including *U. hordei* and *M. pennsylvanicum* (Hemetsberger *et al.*, 2015). Another core effector crucial for virulence is Cce1 (Seitner *et al.*, 2018). Cce1 possesses similar features as Pep1, e.g. is a protein of only 129 amino acids and possesses eight cysteine residues. Its virulence-promoting function can be complemented by the ortholog from *U. bromivora* (Seitner *et al.*, 2018). Although the function of Cce1 is still unclear, the authors speculate that Cce1 may also inhibit early plant defense responses in the apoplast. A third apoplastic core effector is Rsp3 and its virulence-promoting function is conserved in the ortholog from *S. reilianum* (Ma *et al.*, 2018). Rsp3 localizes at the surface of fungal cells and protects them from the maize antifungal proteins AFP1 and AFP2 (Ma *et al.*, 2018). These three examples illustrate that core effectors of *U. maydis* have important virulence functions.

In this study, we identified the *sta1* as a novel core effector gene in *U. maydis* that is transiently upregulated during the early infection stages and is required for virulence. To carry out its virulence function, *sta1* expression needs to occur during a specific time window after plant colonization. Sta1 is a cell wall protein specifically attached to hyphae and likely needed to re-organize the fungal cell wall structure at a specific stage during host colonization.

Materials and Methods

Growth conditions and virulence assays

Zea mays cv. Early Golden Bantam (Urban Farmer, Westfield, Indiana, USA) was used to assess virulence of *U. maydis*. Plants were grown in a temperature-controlled greenhouse (14/10 h light (15,000 lux)/dark cycle; 28 °C/20 °C). The solopathogenic strain SG200 and haploid strains FB1 and FB2 of *U. maydis* have previously been described (Banuett & Herskowitz, 1989; Kamper *et al.*, 2006). For virulence assay, *U. maydis* strains were grown in YEPSL (0.4% yeast extract, 0.4% peptone, 2% sucrose) on a rotary shaker (200 r.p.m.) at 28 °C overnight. Cells were pelleted and resuspended in H_2O (OD_{600} = 1.0) and then injected into the stem of 7 day-old maize seedlings with a syringe as

previously described (Kamper *et al.*, 2006). Disease symptoms were scored at 12 days post infection using a previously developed scoring scheme (Kamper *et al.*, 2006). Disease symptoms were quantified based on three biological replicates, and are presented as stacked histograms. The raw data of all infection assays as well as the statistical analysis can be found in Table S1. Teliospore germination was performed as previously described (Flor-Parra *et al.*, 2007).

Plasmid construction and mutant generation

Either the Gibson Assembly kit (New England Biolabs, Frankfurt am Main, Germany) or standard molecular cloning techniques were used for plasmid construction. DNA assembly using the Gibson Assembly kit was performed according to the manufacturer's protocol. All plasmids generated or used in this study are listed in Table S2. All primers used for DNA amplification are listed in Table S3.

To generate deletion mutants of *sta1* (*UMAG_12226*) in *U. maydis*, the deletion construct pKO_HygR_sta1 was generated. The left and right border regions (1000 bp each) of *sta1* were amplified by polymerase chain reaction (PCR) with primers Um12226_LB_Gib-F and Um12226_LB_Gib-R, and Um12226_RB_Gib-F and Um12226_RB_Gib-R, respectively. Amplified fragments were mixed with a hygromycin resistance marker cassette amplified with primers Um12226_RB_Gib-F and Um12226_RB_Gib-R from plasmid pBS-Hyg (Molina & Kahmann, 2007) and pBlueScript linearized by *Eco*RI-*Bam*HI, and were assembled using the Gibson Assembly kit. From the resulting plasmid, a 4 kb *Ssp*I fragment containing the hygromycin resistance marker cassette flanked by the left and right border regions of *sta1* was used for transformation of *U. maydis* SG200, FB1 and FB2 strains. Gene replacement mutants were identified by Southern blot analysis.

To generate a complementation strain of SG200Δsta1, the construct p123_Sta1 was generated. Genomic DNA from SG200 containing promoter and open reading frame of *sta1* were amplified by PCR with primers um12226pro-F and um12226-R. The amplified fragment was introduced into the integrative plasmid p123 (Aichinger *et al.*, 2003) after digestion by *Nde*I and *Asc*I. To complement the virulence defects of SG200Δsta1 by Sta1-HA, the construct p123_Sta1_HA was generated. Genomic DNA from SG200 containing promoter and open reading frame of *sta1* were amplified by PCR with primers um12226pro-F and um12226-R2. The amplified fragment was introduced into p123 as described above. To generate a strain where Sta1 fused with mCherry-HA is expressed from

its own promoter, the plasmid p123_Sta1_mCherry_HA was generated as follows. From genomic DNA of SG200, *sta1* including promoter and open reading frame was amplified with primers um12226pro_Gib-F and um12226_Gib-R. *mCherry* was amplified by PCR with primers mCherry_HA_Gib-F and mCherry_HA_Gib-R from plasmid p35S-Tin2$_{26–207}$-mCherry-HA-3xNLS (Tanaka *et al.*, 2015a). Amplified fragments were assembled using the Gibson Assembly kit into p123 linearized by *Kpn*I-*Not*I. Prior to transformation, plasmids were linearized with *Ssp*I. Transformants were screened by southern analysis and strains were chosen in which a single copy of the plasmid was inserted in the *ip* locus of SG200Δsta1 (Loubradou et al, 2001)

To generate complementation strains of SG200Δsta1 by *sta1* orthologs from other smut pathogens, the 323 bp promoter region of *U. maydis sta1* and open reading frame of *sta1* orthologs from other smut pathogens were amplified by PCR with the primers indicated in Table S2 using genomic DNA from *U. hordei* strain 4875-4, *S. reilianum* SRZ5-1, *S. scitamineum* SscI8, and *M. pennsylvanicum* MP4, respectively. Amplified fragments were assembled using the Gibson Assembly kit into *Kpn*I-*Not*I linearized p123. To generate a complementation construct for the *sta1* ortholog from *T. cyperi*, a synthetic gene codon-optimized for *U. maydis* was generated (Eurofins Genomics, Ebersberg, Germany) and fused with the 323 bp promoter region of *U. maydis sta1* in p123 as described above. Transformants containing a single copy of *Ssp*I linearized complementation constructs inserted in the *ip* locus of SG200Δsta1 were identified as previously described (Loubradou *et al.*, 2001).

To generate a strain where cytosolic mCherry-HA is expressed from the *sta1* promoter, the plasmid p123_P$_{sta1}$_mCherry_HA was generated as follows. From genomic DNA of SG200, the *sta1* promoter was amplified with primers um12226proGib-F4 and um12226pro_Gib-R4. *mCherry-HA* was amplified by PCR with primers mCherry_HA_Gib-F2 and mCherry_HA_Gib-R2 from p35S-Tin2$_{26–207}$-mCherry-HA-3xNLS (Tanaka *et al.*, 2015a). Amplified fragments were assembled using the Gibson Assembly kit into *Kpn*I-*Not*I linearized p123. p123_P$_{sta1}$_mCherry_HA was linearized with *Ssp*I and inserted into the *ip* locus of SG200Δsta1 as described (Loubradou *et al.*, 2001).

To express Sta1-3xHA or Tin2-3xHA protein constitutively in *U. maydis*, plasmids p123_P$_{actin}$_Sta1_3xHA and p123_P$_{actin}$_Tin2_3xHA were generated as follows. The plasmid pDL252 containing 2 kb upstream region of the *U. maydis* actin gene (*UMAG_11232*) (D. Lanver and R. Kahmann, unpublished) was digested with *Nco*I-*Asc*I. From genomic DNA of SG200, the *sta1* or *tin2*

genes were amplified by PCR with primers um12226ORF-F and um12226ORF-R, and tin2ox-F2 and tin2entry-R, respectively. Amplified fragments were assembled using the Gibson Assembly kit and introduced into *Nco*I-*Asc*I sites downstream of the actin promoter. p123_P_{actin}_Sta1_3xHA and p123_P_{actin}_Tin2_3xHA were linearized with *Age*I and inserted in single copy into the *ip* locus of SG200Δsta1 as described (Loubradou *et al.*, 2001).

To generate a strain where mCherry-HA carrying a signal peptide is expressed from the *sta1* promoter, the plasmid p123_P_{sta1}_SP_mCherry_HA was generated as follows. From genomic DNA of SG200, the region containing the *sta1* promoter and signal peptide was amplified with primers um12226proGib-F4 and um12226proGib-R6. *mCherry-HA* was amplified by PCR with primers mCherry_HA_Gib-F3 and mCherry_HA_Gib-R from plasmid p35S-Tin2$_{26–207}$-mCherry-HA-3xNLS (Tanaka *et al.*, 2015a). Amplified fragments were assembled using the Gibson Assembly kit into *Kpn*I-*Not*I linearized p123. p123_P_{sta1}_SP_mCherry_HA was linearized with *Ssp*I and inserted in single copy into the *ip* locus of SG200Δsta1 as described (Loubradou *et al.*, 2001).

To generate complementation strains of SG200Δsta1 by *sta1* under the *UMAG_04033* promoter, the 685 bp promoter region of *UMAG_04033* and open reading frame of *sta1* were amplified from SG200 genomic DNA by PCR with the primers um04033pro_Gib-F and um04033pro_Gib-R, and um12226ORF_Gib-F and um12226ORF_Gib-R, respectively. Amplified fragments were assembled using the Gibson Assembly kit into *Kpn*I-*Not*I linearized p123 to yield p123_P_{UMAG_04033}_Sta1. p123_P_{UMAG_04033}_Sta1 was linearized with *Ssp*I and inserted in single copy into the *ip* locus of SG200Δsta1 as described (Loubradou *et al.*, 2001). All strains used in this study are listed in Table S4.

Confocal microscopy

The proliferation of *U. maydis* in infected maize leaf tissue was visualized by confocal microscopy as previously described (Tanaka *et al.*, 2014). One cm of leaf area located 2 cm below the injection hole was excised at 2 days post infection. Leaf samples were destained by ethanol and treated with 10% (w/v) KOH at 85 °C for 4 h. Fungal hyphae were stained with Wheat Germ Agglutinin-Alexa Fluor 488 (WGA-AF488; Invitrogen, Karlsruhe, Germany). Plant cell walls were stained with propidium iodide (Sigma-Aldrich, Schnelldorf, Germany) by incubating decolorized samples in staining solution (1 µg ml^{-1} propidium iodide, 10 µg ml^{-1} WGA-AF488) and observed with a TCS-

SP8 confocal laser-scanning microscope (Leica Microsystems, Wetzlar, Germany) under the following conditions; WGA-AF488: excitation at 488 nm and detection at 500-540 nm; propidium iodide: excitation at 561 nm and detection at 580-660 nm. To visualize mCherry fusion proteins in the infected maize tissue, plant tissues were directly observed with a TCS-SP8 (Leica Microsystems, Wetzlar, Germany) as previously described (Tanaka *et al.*, 2015a); excitation at 561 nm and detection at 580-630 nm. Plasmolysis was performed as previously described (Tanaka *et al.*, 2014). Fungal plasma membrane was visualized after treatment with 10 μM FM4-64 (Thermo Fisher Scientific, Dreieich, Germany) for 10 min followed by excitation at 514 nm and detection at 650-700 nm. To prepare leaf cross sections, 1 cm x 1 cm regions of infected leaf area were embedded in 5% (w/v) low gelling temperature agarose (Sigma-Aldrich, Schnelldorf, Germany; A9414). Embedded samples were cut at 80 μm thickness by a Leica VT1000S Vibrating Blade microtome (Leica Microsystems, Wetzlar, Germany). Leaf cross sections were directly observed by a TCS-SP5 confocal laser-scanning microscope (Leica Microsystems, Wetzlar, Germany). Plant cell walls were visualized by autofluorescence (excitation at 405 nm and detection at 420-470 nm). Fungal hyphae were visualized by WGA-AF488 staining as described above.

qRT-PCR analysis

Total RNA was extracted with TRIzol reagent (Thermo Fisher Scientific, Dreieich, Germany) from infected maize leaves with SG200 or SG200Δsta1 at 2 dpi by excising 2–3 cm segments from below the injection holes. At least 15 leaf segments were pooled and ground into a fine powder using a mortar/pestle under liquid nitrogen. Quantitative real-time PCR reactions were performed as previously described (Tanaka *et al.*, 2014). All reactions were performed with three biological replicates. Relative gene expression in infected leaf tissues was calculated in relation to the values obtained for *GAPDH* of *Z. mays*. Fungal biomass was determined as previously described (Brefort *et al.*, 2014). Primers used for qRT-PCR are listed in Table S3.

Western blot analysis

Hemagglutinin (HA)-tagged proteins in infected leaf extracts were detected as previously described (Tanaka *et al.*, 2014; Tanaka *et al.*, 2019). For immunoprecipitation, 5 ml culture supernatant or

protein extract from infected leaf tissue was incubated with 20 µl monoclonal anti-HA−Agarose antibody produced in mouse (Sigma-Aldrich, Schnelldorf, Germany) at 4°C for 2 hr on a rotary shaker. Bound proteins were eluted from the beads by heating to 99 °C for 10 min. Proteins were separated by 12% SDS–polyacrylamide gel electrophoresis. A rabbit polyclonal anti-haemagglutinin antibody (Sigma-Aldrich, Schnelldorf, Germany) was used as the primary antibody at 1:10,000 dilution. Anti-rabbit IgG horseradish peroxidase-linked antibody (Cell Signaling Technology, Leiden, the Netherlands) was used as a secondary antibody at 1:10,000 dilution. To detect signals, SuperSignal West Femto Maximum Sensitivity Substrate (Thermo Fisher Scientific, Dreieich, Germany) was used as substrate for horseradish peroxidase and the signal was visualized by exposure to X-ray film.

Immunostaining

To visualize the localization of Sta1-3xHA protein on the surface of fungal cells, immunostaining was performed as previously described (Ma *et al.*, 2018). *U. maydis* strains constitutively expressing Sta1-3xHA or Tin2-3xHA were suspended in 2% YEPSL containing 0.1 mM 16-hydroxy hexadecanoic acid at OD_{600} = 0.5 and sprayed onto parafilm to induce filamentation (Mendoza-Mendoza *et al.*, 2009). The parafilm was incubated at 28 °C for 16 h. After washing with phosphate-buffered saline (PBS), parafilm was incubated in PBS containing mouse anti-HA antibody (Sigma-Aldrich, Schnelldorf, Germany; 1:1,500 dilution) and 3% bovine serum albumin at 4 °C overnight. After washing, parafilm was incubated in PBS containing goat anti-mouse IgG secondary antibody conjugated with Alexa Fluor 488 (Life Technologies, Darmstadt, Germany; 1:1,500 dilution) for 1 h at room temperature. After washing, the samples were analyzed using a TCS-SP8 confocal laser-scanning microscope (Leica Microsystems, Wetzlar, Germany).

Fungal stress assay

The strains were grown in YEPSL until an OD_{600} = 1.0. Cells were pelleted and resuspended in H_2O to OD_{600} = 0.1. Ten µl of serial dilutions were spotted on PD-charcoal plates to induce filament formation. Stress plates were PD-charcoal plates (Krombach *et al.*, 2018) supplemented with 1 mg ml^{-1} Congo red (Sigma-Aldrich, Schnelldorf, Germany), 750 µM Calcofluor white (Sigma-Aldrich,

Schnelldorf, Germany), 0.0625% (w/v) SDS or 3 mM H_2O_2. Compared to previous stress assays performed on PD-plates (Krombach *et al.*, 2018), higher concentrations of the stressors needed to be added to PD-plates containing activated charcoal. For chitinase and β-glucanase assay, 10 µg µl^{-1} of chitinase (Sigma-Aldrich, Schnelldorf, Germany; C6137) or 100 µg µl^{-1} of β-1,3-glucanase (Sigma-Aldrich, Schnelldorf, Germany; 67138) were prepared in PBS (pH 7.2) or 150 mM sodium acetate buffer (pH 5.0), respectively. Specific activity of chitinase was >200 units/g (one unit liberates 1.0 mg of N-acetyl-D-glucosamine from chitin per hour) and β-1,3-glucanase was >200 units/g (one unit liberates 1 µmol of glucose from laminarin per minute). One µl of chitinase solution or β-1,3-glucanase solution was directly spotted onto filamentous colonies formed 24 hrs after spotting 10 µl of cell suspension on PD-charcoal plates as described above. After overnight incubation, the colonies were observed by a Leica M165FC stereomicroscope (Leica Microsystems, Wetzlar, Germany).

Accession numbers

The genes and encoding protein sequences from *U. maydis* and other smut pathogens are available at NCBI under the following accession numbers: *U. maydis sta1* (*UMAG_12226*), XP_011389862.1; *Sporisorium reilianum Srsta1*(*Sr14368*), SJX63616.1; *Sporisorium scitamineum Scsta1*(*SPSC_04422*), CDS00967.1; *Ustilago hordei Uhsta1*(*UHOR_05232*), CCF52074.1; *Ustilago bromivora Ubsta1*(*UBOR_05232*), SAM82532.1; *Testicularia cyperi TcSta1*(BCV70DRAFT_217309), PWZ00322.1. The ortholog of *sta1* in *M. pennsylvanicum* (*MpSta1*, *MEPE_03556*) was detected after PacBio resequencing and reannotation of strain MP4 (Sharma *et al.*, 2014) (M. Schuster, G. Schweizer, S. Tanaka, G. Mannhaupt and R. Kahmann, unpublished).

Results

Identification of Sta1 as a novel virulence-promoting effector in *U. maydis*

To identify novel virulence effector genes in *U. maydis*, we focused on gene conservation in several smut species and the expression pattern during plant colonization (Lanver *et al.*, 2018). *UMAG_12226* encodes a putative novel secreted protein and RNA-seq data indicate that the gene is specifically upregulated during the early stages of plant infection when biotrophic development is established (Fig.

1a). *UMAG_12226* encodes a protein of 169 amino acids (18.9 kDa) carrying a signal peptide at the N-terminus predicted by SignalP5.0 (Almagro Armenteros *et al.*, 2019) (Fig. 1b). The protein contains eight cysteine residues without any known motifs or domains (Fig. 1b). To analyze whether *UMAG_12226* contributes to virulence, we generated deletion mutants of *UMAG_12226* in the solopathogenic strain SG200 of *U. maydis* and performed virulence assays. The deletion mutants of *UMAG_12226* showed a severe reduction of virulence (Fig. 1c), although anthocyanin induction, which is indicative of biotrophic growth, was not impaired (Fig. 1c). The ability to induce large and normal size tumors was most significantly impaired in the mutants and tumors formed were generally small (< 1 mm in diameter) or developed only in ligula tissue (Fig. 1d). Therefore, we designated *UMAG_12226* as *sta1* (small tumor-associated 1). The introduction of the *sta1* gene in single copy in the *ip* locus of SG200Δsta1 fully complemented all virulence defects (Fig. 1c). Complementation of the deletion mutant was also observed when Sta1 was fused with either a hemagglutinin (HA) epitope tag or mCherry at the C-terminus (Fig. 1d), illustrating functionality of these fusion proteins. In addition, we also generated *sta1* mutants in compatible haploid *U. maydis* strains FB1 and FB2, which infect via dikaryotic hyphae. Similar to SG200Δsta1, the cross of FB1Δsta1 x FB2Δsta1 showed a dramatic reduction of tumor formation in leaf tissue (Fig. S1a,b). However, we could observe tumor development in the stem of infected maize seedlings (categorized as “Heavy tumors”; Fig. S1a,b) and such tumors contained teliospores, which were able to germinate (Fig. S1c,d). This indicates that the *sta1* deletion mutants can complete the sexual life cycle.

Host colonization and tumor development are altered when *sta1* is deleted

To detect differences in host colonization between SG200 and SG200Δsta1, we visualized fungal hyphae by staining with WGA-AF488 at 2 dpi, when the expression of *sta1* reaches its maximum. At this time point, hyphae of SG200 had colonized leaf epidermal cells, passed through mesophyll tissue and reached the bundle sheath cells in vascular structures. However, at 2 and 4 dpi we could neither observe significant differences of fungal colonization between SG200 and SG200Δsta1 by confocal microscopy (Fig. S2a) nor in biomass (Fig. S2b). When fungal structures in infected leaf tissue were visualized by three-dimensional confocal microscopy, it was apparent that SG200 hyphae in discrete vascular bundles were connected (Fig. 2a). In SG200Δsta1, the fungal hyphae had also colonized leaf

epidermal cells and reached the bundle sheath cells (Fig. 2a). However, hyphae of SG200Δsta1 in vascular bundles were rarely connected to hyphae in neighboring vascular bundles (Fig. 2a). This suggests that Sta1 is likely to be needed for efficient colonization of tissue adjacent to the vasculature. Next, we prepared leaf cross sections of plants infected with SG200, SG200Δsta1 and H_2O as mock control at 6 dpi, when tumor formation is apparent. In tumor tissue colonized by SG200, mesophyll cells were enlarged and bundle sheath cells had largely disappeared due to resumed cell division and endoreduplication (Fig. 2b) as described before (Matei *et al.*, 2018). In contrast, in SG200Δsta1-infected leaf area lacking tumors, the structure and size of mesophyll cells were similar to the mock control and bundle sheath cells were unaltered (Fig. 2b). In addition, we found that the cell wall of mesophyll cells infected by SG200Δsta1 showed stronger autofluorescence compared to those infected by SG200 (Fig. 2b). We also compared autofluorescence in SG200-infected leaf areas lacking tumors to corresponding areas infected by SG200Δsta1 (Fig. S3a). Here we could observe stronger autofluorescence in SG200Δsta1-infected tissue than in SG200-infected tissue (Fig. S3b). As this could suggest plant cell wall fortifications, we next analyzed by qRT-PCR the expression of diagnostic genes from the phenylpropanoid pathway in plants infected with either SG200 or SG200Δsta1 at 2 dpi. This analysis revealed that the 4-coumarate CoA ligase (4CL) genes as well as cinnamyl alcohol dehydrogenase (CAD) gene were significantly upregulated after infection with SG200Δsta1 (Fig. S4). The upregulation of these genes could indicate enhanced lignification.

Sta1 is functionally conserved in related smut fungi

A search for orthologs of *sta1* in pathogenic smut fungi whose genome sequences are publicly available revealed presence in the smut fungi *Sporisorium reilianum*, *Sporisorium scitamineum*, *Ustilago hordei*, *Ustilago bromivora*, *Ustilago tritici, Ustilago esculenta* and *Ustilago trichophora* (Fig. S5), which all belong to the Ustilaginaceae family (Schirawski *et al.*, 2010; Laurie *et al.*, 2012; Dutheil *et al.*, 2016; Rabe *et al.*, 2016; Zambanini *et al.*, 2016; Ye *et al.*, 2017; Benevenuto *et al.*, 2018). The sequence identity of these orthologs with Sta1 from *U. maydis* ranges between 46.15 - 60.35 % (Table S5). Initially a *sta1* ortholog could not be found in the genome of dicot smut *Melanopsichium pennsylvanicum* (Sharma *et al.*, 2014), but was detected after PacBio resequencing and reannotation of the *M. pennsylvanicum* genome (M. Schuster, G. Schweizer, S. Tanaka, G.

Mannhaupt and R. Kahmann, unpublished). In all orthologs, six of the eight cysteine residues are present and their spacing is conserved (Fig. S5). A protein related to Sta1 was also found in *Testicularia cyperi*, which infects *Rhynchospora* spp. and belongs to the family Anthracoideaceae (Fig. S5) (Kijpornyongpan *et al.*, 2018). Although the sequence identity with *U. maydis* Sta1 is only 30.17 % (Table S5), five of the eight cysteine residues are conserved (Fig. S5). In Ustilaginaceae, the *sta1* gene loci are highly syntenic, although in *M. pennsylvanicum* the distance between *sta1* and the neighboring gene on the left is extended (Fig. 3a). An extension of the region between *sta1* and the neighboring gene on the left is also seen in *T. cyperi* (Fig. 3a). In the *Brassicaceae*-infecting smut *Thecaphora thlaspeos*, belonging to the family Glomosporiaceae that is considered as a sister taxon of the order Urocystales (Vanky *et al.*, 2008; Courville *et al.*, 2019), an ortholog of *sta1* could not be detected. In a phylogenetic analysis, *T. thlaspeos* is placed distantly from the other plant pathogenic smuts (Fig. 3b) and the region between orthologous neighboring genes to the left (*UMAG_11014* in *U. maydis*) and right (*UMAG_03371* in *U. maydis*) is extended to >100 kb (Fig. 3a).

To investigate whether orthologs are functionally conserved, the *U. maydis sta1* deletion mutant was complemented by introducing orthologs from *S. reilianum*, *S. scitamineum*, *U. hordei* and *M. pennsylvanicum*. All genes were expressed from the *sta1* promoter of *U. maydis* in SG200Δsta1. All orthologs tested could fully complement the virulence phenotype of the *sta1* mutant (Fig. 3c). To examine whether Sta1 function is also conserved in the more distantly related smuts, we complemented SG200Δsta1 by the gene from *T. cyperi*. In contrast to the orthologs from Ustilaginaceae, we detected only partial complementation in two independent complementation strains (Fig. 3d). This result indicates that the function of Sta1 proteins is fully conserved in Ustilaginaceae smut pathogens while the more distantly related Sta1 protein from *T. cyperi* shows partial functional divergence.

Secreted Sta1 protein is detected on hyphal cell walls

We studied the localization of Sta1-mCherry-HA protein expressed under the *sta1* promoter during leaf infection by confocal microscopy. Here we could observe mCherry fluorescence around biotrophic hyphae, while the fluorescence from a strain expressing cytosolic mCherry-HA under the *sta1* promoter accumulated inside fungal cells (Fig. 4a). To visualize whether Sta1 protein resides in

the apoplast or is attached to hyphae, we also performed plasmolysis of leaf tissues infected with strains expressing secreted mCherry-HA, Sta1-mCherry-HA or cytosolic mCherry-HA. Plasmolysis should release the plant plasma membrane from the plant cell wall and from hyphae, which are encased by the plant plasma membrane (Doehlemann *et al.*, 2009). Without plasmolysis, secreted mCherry-HA was located in the region surrounding fungal hyphae (Fig. S6), because biotrophic hyphae are encased by the host plasma membrane. However, due to diffusion of secreted mCherry-HA into apoplastic space the fluorescence disappeared after plasmolysis (Fig. S6). Cytosolic mCherry-HA was detected in hyphae also after plasmolysis (Fig. S6). In contrast, Sta1-mCherry-HA was detectable on the surface of fungal hyphae also after plasmolysis (Fig. S6), indicating binding of Sta1 to hyphae.

We generated the strain SG200Δsta1:P_{actin}-Sta1-3xHA that constitutively expresses Sta1-3xHA under the actin promoter and immunoprecipitated Sta1-3xHA protein from culture supernatants. Note that the expression level of the actin promoter is approximately three times higher than the maximum expression level of the *sta1* promoter (Lanver et al., 2018). A signal at the expected size of Sta1-3xHA protein (20.71 kDa without signal peptide) was detected (Fig. 4b), showing that Sta1 can be secreted. To investigate whether Sta1-HA produced by biotrophic hyphae of SG200Δsta1:Sta1-HA after colonization is detectable at the expected size, we attempted to immunoprecipitate Sta1-HA protein from leaf tissue infected with SG200Δsta1:Sta1-HA. However, we failed to detect Sta1-HA protein when total protein was extracted by a buffer lacking SDS (Fig. 4c). Using the same extraction buffer after infection with SG200Δsta1:P_{sta1}-SP-mCherry-HA, mCherry-HA protein could be detected in such extracts (Fig. 4c). However, when the extraction buffer contained 0.1 % SDS, full length Sta1-HA and Sta1-mCherry-HA as well as degradation products could be detected after immunoprecipitation (Fig. 4d). These results suggest that Sta1 protein is attached to biotrophic hyphae.

Next we attempted immunostaining of Sta1-HA in non-permeabilized budding cells or filamentous cells of SG200Δsta1:P_{actin}-Sta1-3xHA induced on parafilm in the presence of hydroxy fatty acids (Mendoza-Mendoza *et al.*, 2009). While we could not detect any fluorescence in budding cells from axenic culture (Fig. 5a), which were previously shown to secrete Sta1-3xHA (Fig. 4b), a strong signal was detected on the surface of filamentous cells on parafilm (Fig. 5b). In contrast, SG200Δtin2:P_{actin}-

Tin2-3xHA did not show a signal (Fig. S7). Tin2 is a translocated effector (Tanaka *et al.*, 2014), which consequently should not bind to the fungal cell wall. Budding cells, which failed to form filaments on parafilm, did not show any signal (Fig. S8). As negative control, filamentation of SG200 was induced with hydroxy fatty acids on parafilm, but in this case no signal could be detected (Fig. 5b). We also showed that budding cells taken from a colony of SG200Δsta1:P_{actin}-Sta1-3xHA grown on a PD plate did not show any fluorescence signal (Fig. S9). Taken together, these results indicate that Sta1 protein specifically attaches to *U. maydis* filaments but fails to bind to budding cells.

Furthermore, we simultaneously visualized Sta1-3xHA protein by immunostaining and the fungal plasma membrane by FM4-64 in non-permeabilized filaments of SG200Δsta1:P_{actin}-Sta1-3xHA. We could observe the Sta1-3xHA signal as well as the FM4-64 signal at the cell periphery but the two signals were not overlapping (Fig. 6a). However, after plasmolysis, the two signals separated and the Sta1-3xHA signal remained at the cell periphery, while the FM4-64 signal was now internalized (Fig. 6b). The latter is characteristic for vesicular uptake, which is a fast reaction taking only minutes (Wedlich-Soldner *et al.*, 2000). These results indicate that Sta1 resides in the hyphal cell wall.

Overexpression of Sta1 protein alters cell wall integrity in filamentous cells

While hydrophobicity of SG200, SG200Δsta1:P_{actin}-Sta1-3xHA and SG200Δtin2:P_{actin}-Tin2-3xHA was indistinguishable (Fig. S10), filaments extending from colonies formed by SG200Δsta1:P_{actin}-Sta1-3xHA were shorter compared to SG200 and SG200Δtin2:P_{actin}-Tin2-3xHA (Fig. 7a), suggesting that filamentous cells of SG200Δsta1:P_{actin}-Sta1-3xHA might have an altered cell wall. To examine whether this results in an altered sensitivity to abiotic stresses, we spotted serial dilutions of SG200, SG200Δsta1:P_{actin}-Sta1-3xHA and SG200Δtin2:P_{actin}-Tin2-3xHA on PD-charcoal plates containing stressors including Congo red, Calcofluor white, H_2O_2 and SDS. While we could not detect significant differences among the three strains in the presence of Calcofluor white, H_2O_2 and SDS (Fig. 7b), SG200Δsta1:P_{actin}-Sta1-3xHA showed a severe reduction of filamentation in the presence of Congo red (Fig. 7b). However, growth of budding cells of these strains was not affected by Congo red on a PD-Congo red plate (Fig. S11).

We also applied a drop of chitinase or β-glucanase solution to the filamentous colonies of SG200, SG200Δsta1:P_{actin}-Sta1-3xHA and SG200Δtin2:P_{actin}-Tin2-3xHA. Filamentous cells of

SG200Δsta1:P_{actin}-Sta1-3xHA were efficiently lysed by chitinase and β-glucanase, while SG200 and SG200Δtin2:P_{actin}-Tin2-3xHA were not (Fig. 7c). Upon chitinase treatment, the filamentous cells of SG200Δsta1:P_{actin}-Sta1-3xHA showed chains of rounded structures (Fig. 7d) while filaments of SG200 were mostly unaffected (Fig. 7d). In contrast, we did not observe these structures after β-glucanase treatment (Fig. S12). Overall, these results indicate that the constitutive expression of Sta1 protein in filaments results in an altered cell wall structure. When yeast-like colonies of the same three strains were treated with chitinase and β-glucanase in the same concentrations as used for filamentous cells, none of the three strains was lysed even when higher concentrations of chitinase and β-glucanase were used (Fig. S13). These results show that constitutive expression of Sta1 influences susceptibility to β-glucanase and chitinase specifically in filamentous cells.

To investigate whether cell wall alterations can also be visualized when comparing SG200 and SG200Δsta1, we first performed RT-PCR on RNA from SG200 filaments grown on a PD-charcoal plate. The *sta1* expression was detectable, while *tin2* effector gene expression was not (Fig. S14a). Filamentous colonies and filaments were not distinguishable between SG200 and SG200Δsta1 (Fig. S14b). Furthermore, we could observe significant differences neither in growth between SG200 and SG200Δsta1 on PD-charcoal plates containing different stressors (Fig. S14c) nor in sensitivity to chitinase and β-glucanase (Fig. S14d). In particular, no differences in sensitivity to Congo red were apparent between SG200 and SG200Δsta1. We consider it likely that SG200 produces only small amounts of Sta1 under these conditions, which does not allow to detect phenotypic differences to SG200Δsta1.

Altered timing of *sta1* expression interferes with the function of Sta1

Since the expression of Sta1 peaks at an early stage of plant infection (Fig. 1a), we hypothesized that Sta1 might be necessary at this specific infection stage. To test this hypothesis, we introduced the *sta1* gene in strain SG200Δsta1 under the *UMAG_04033* promoter that is induced at a later infection stage (with maximum expression after 8 days post infection) but shows an expression level similar to *sta1* (Fig. 8a). Two independent SG200Δsta1 derivatives expressing *sta1* under this late promoter did not show complementation of virulence (Fig. 8b). To examine whether constitutive expression of Sta1 influences virulence, we also performed virulence assay of SG200Δsta1:P_{actin}-Sta1-3xHA. In this

strain, we observed only weak complementation of virulence (Fig. S15). These results suggest that Sta1 function is needed specifically in a certain time window during infection.

Discussion

In this study, we have characterized the virulence-promoting Sta1 effector as a protein that needs to be expressed in a short time window during plant colonization and specifically attaches to fungal hyphae. We found that Sta1 orthologs exist in all Ustilaginaceae but also in *T. cyperi*, a fungus belonging to the distantly related Anthracoideaceae family in the order Ustilaginales (Kijpornyongpan *et al.*, 2018). However, while four orthologs from Ustilaginaceae fully complemented the virulence phenotype of *U. maydis sta1* mutants, the *T. cyperi* ortholog could only partially complement, suggesting functional divergence. Our finding of partial complementation by the *T. cyperi* ortholog of *sta1* is the first example for functional effector complementation from such a distantly related species, suggesting an ancient function of this effector.

In contrast to secreted proteins that bind to cell wall polysaccharides in other plant pathogenic fungi (van den Burg *et al.*, 2006; de Jonge *et al.*, 2010; Marshall *et al.*, 2011; Mentlak *et al.*, 2012; Takahara *et al.*, 2016), Sta1 does not contain any characterized domains or motifs that implicate carbohydrate binding. At this point, we cannot exclude the possibility that Sta1 might bind to another protein whose expression occurs in the filamentous form only. Currently only two proteins of this class are known. One is the repellent protein Rep1, which provides for surface hydrophobicity but is not needed for virulence (Wosten *et al.*, 1996) and is therefore unlikely to be a binding partner for Sta1. A second protein is Rsp3, a virulence-promoting effector that does not contain a carbohydrate-binding domain but localizes to the fungal cell wall. However, in this case both budding cells and filamentous cells were decorated by Rsp3 when Rsp3 was constitutively expressed (Ma *et al.*, 2018). As the native expression pattern of *rsp3* is similar to the *sta1* (Lanver *et al.*, 2018; Ma *et al.*, 2018), Rsp3 could be the binding partner of Sta1. To show this, one could express Sta1 in budding cells constitutively expressing Rsp3 and analyze whether such cells display attached Sta1 protein. Another possibility is that Sta1 binds to carbohydrate in the cell wall of *U. maydis*. Although the cell wall composition in budding cells and filamentous cells induced after mating of *U. maydis* has not been analyzed in detail,

it is known from other plant pathogenic fungi that they alter their cell wall composition during colonization. The rust fungi *Puccinia graminis* f. sp. *tritici* and *Uromyces fabae*, as well as the ascomycete plant pathogens *Colletotrichum graminicola* and *Magnaporthe oryzae* use chitin deacetylases to convert chitin to chitosan in the cell wall of infection structures (El Gueddari *et al.*, 2002; Fujikawa *et al.*, 2009). *U. maydis* encodes several chitin deacetylases (Ruiz-Herrera *et al.*, 2008) and it is therefore conceivable that biotrophic hyphae have an altered cell wall structure compared to budding cells and contain chitosan. Chitosan could then become the natural substrate of Sta1 during infection. So far the function of these enzymes has not been characterized in *U. maydis* and it is unknown whether they contribute to virulence. In future one could attempt constitutive expression of chitin deacetylases in budding cells, demonstrate that chitin is converted to chitosan in the cell wall with the help of a chitosan-affinity protein (Nampally *et al.*, 2012) and reveal if this might allow binding of Sta1. Filaments of an *U. maydis* strain that constitutively express Sta1 protein show increased susceptibility to the fungal cell wall inhibitor Congo red (Ram & Klis, 2006). Congo red is thought to bind to chitin and interfere with β-glucan synthesis (Kopecka & Gabriel, 1992; Ram & Klis, 2006), which may affect the formation of covalent links between chitin chains and β-glucan (Ram & Klis, 2006). The increased sensitivity to Congo red suggests that the attachment of Sta1 protein to the cell wall has altered the cell wall properties of hyphae. In line with this, we observed that filaments that constitutively express Sta1 also show increased susceptibility to chitinase and β-glucanase, which are enzymes degrading chitin and β-glucan respectively. This makes it likely that Sta1 has altered the cell wall structure or has increased accessibility of the chitin and glucan layer to attack by these enzymes. However, we cannot formally rule out the possibility that the increased susceptibility to these enzymes is due to the about 3-fold higher than native expression of Sta1 conferred by placing *sta1* under the actin promoter. In contrast to chitinase, which induced changes to intracellular structure, β-glucanase treatment did not induce such a structural phenotype in filaments constitutively expressing Sta1. We speculate that disruption of the inner chitin layer triggers a much more severe stress response than the response triggered by removal of β-glucan in the outer layer of the fungal cell wall as previously reported in filaments of another basidiomycete fungus (Mogilnaya *et al.*, 2017).

The peak of *sta1* expression is at 2 dpi, a time point prior to tumor development in leaf tissue, and subsequently *sta1* expression levels decrease gradually as fungal infection progresses. When *sta1* was expressed from a late promoter (expression peak at 8 dpi), or when *sta1* was constitutively expressed, the virulence-promoting function was compromised, suggesting that correct timing of *sta1* expression is necessary. This could reflect that attachment of Sta1 protein to hyphae already during penetration might increase vulnerability of fungal hyphae to plant-derived cell wall degrading enzymes. Maize chitinases and β-glucanases are upregulated during early colonization stages but downregulated at 24 hpi and later time points (Doehlemann *et al.*, 2008), which is likely achieved by secreted effectors. In this respect it would be interesting to analyze whether the strongly reduced virulence of the strain constitutively expressing *sta1* is caused by developmental defects of hyphae in epidermal tissue.

The proposed benefit of cell wall modification by attachment of Sta1 protein to hyphae of *U. maydis* when expressed from the native promoter is not clear yet. With respect to growth, the *sta1* mutant was comparable to wild type at 2 dpi, suggesting that the mutant does not have critical morphological defects and appears fit for survival in leaf tissue. However, detailed confocal microscopy found that biotrophic hyphae of the *sta1* mutant had reached the vascular bundles but were less efficient in spreading to regions between vascular bundles. This could suggest that mutant hyphae, which lack Sta1 protein on the surface, might be recognized and elicit defense responses in this specific plant cell type. Transcriptional analysis in mesophyll cells and bundle sheath cells upon *U. maydis* infection demonstrated that the different plant cell type shows different gene expressions (Villajuana-Bonequi *et al.*, 2019), suggesting the possibility that specific plant cell types may show specific plant defense responses. In this scenario, Sta1 might protect hyphae or prevent release of cell wall fragments eliciting these defense responses. Plant defense responses are often associated with a reinforcement of the plant cell wall (Huckelhoven, 2007; Underwood, 2012). If the increased autofluorescence and upregulation of genes from the phenylpropanoid pathway after infections with the *sta1* mutant is indicative for enhanced lignification, this might also explain why *sta1* mutants fail to induce the enlargement of mesophyll cells, fail to induce endoreduplication of bundle sheath cells (Matei *et al.*, 2018) and fail to spread between infected vascular bundles. However, since there is a little disconnection of the time line of the events between the transcriptional pattern of the *sta1* gene and

the phenotype observed, we cannot exclude the possibility that the mutant effects seen are of secondary nature.

These studies have allowed us to classify Sta1 as a novel type of effector that can bind specifically to *U. maydis* hyphae, and which likely needs to be bound to hyphae at a specific developmental stage during plant colonization. We speculate that this may go along with alterations in fungal cell wall properties that prevent the elicitation of plant defense responses in a defined tissue type and time window after infection.

Acknowledgements

We are very grateful to Xiaowei Han for critical reading of the manuscript and constructive comments, and to the entire group in Marburg for helpful discussions. We thank Jer-Sheng Lin for supporting the preparation of leaf cross section. We also thank Seán Murray for language correcting in the manuscript. Our work was supported by generous funds from the Max Planck Society.

Author contributions

ST designed and performed experiments. IG performed immunostaining. NR generated strains and performed virulence assay. ST and RK directed the project. ST and RK wrote the manuscript with input from all co-authors.

References

Aichinger C, Hansson K, Eichhorn H, Lessing F, Mannhaupt G, Mewes W, Kahmann R. 2003. Identification of plant-regulated genes in *Ustilago maydis* by enhancer-trapping mutagenesis. *Molecular Genetics and Genomics* **270**(4): 303-314.

Almagro Armenteros JJ, Tsirigos KD, Sonderby CK, Petersen TN, Winther O, Brunak S, von Heijne G, Nielsen H. 2019. SignalP 5.0 improves signal peptide predictions using deep neural networks. *Nature Biotechnology* **37**(4): 420-423.

Banuett F. 1995. Genetics of *Ustilago maydis*, a fungal pathogen that induces tumors in maize. *Annual Review of Genetics* **29**: 179-208.

Banuett F, Herskowitz I. 1989. Different *a* alleles of *Ustilago maydis* are necessary for maintenance of filamentous growth but not for meiosis. *Proceedings of the National Academy of Sciences, USA* **86**(15): 5878-5882.

Benevenuto J, Teixeira-Silva NS, Kuramae EE, Croll D, Monteiro-Vitorello CB. 2018. Comparative genomics of smut pathogens: insights from orphans and positively selected genes into host specialization. *Frontiers in Microbiology* **9**: 660.

Brefort T, Tanaka S, Neidig N, Doehlemann G, Vincon V, Kahmann R. 2014. Characterization of the largest effector gene cluster of *Ustilago maydis*. *PLoS Pathogens* **10**(7): e1003866.

Courville KJ, Frantzeskakis L, Gul S, Haeger N, Kellner R, Hessler N, Day B, Usadel B, Gupta YK, van Esse HP, et al. 2019. Smut infection of perennial hosts: the genome and the transcriptome of the Brassicaceae smut fungus *Thecaphora thlaspeos* reveal functionally conserved and novel effectors. *New Phytologist* **222**(3): 1474-1492.

de Jonge R, van Esse HP, Kombrink A, Shinya T, Desaki Y, Bours R, van der Krol S, Shibuya N, Joosten MH, Thomma BP. 2010. Conserved fungal LysM effector Ecp6 prevents chitin-triggered immunity in plants. *Science* **329**(5994): 953-955.

Doehlemann G, Hemetsberger C. 2013. Apoplastic immunity and its suppression by filamentous plant pathogens. *New Phytologist* **198**(4): 1001-1016.

Doehlemann G, van der Linde K, Assmann D, Schwammbach D, Hof A, Mohanty A, Jackson D, Kahmann R. 2009. Pep1, a secreted effector protein of *Ustilago maydis*, is required for successful invasion of plant cells. *PLoS Pathogens* **5**(2): e1000290.

Doehlemann G, Wahl R, Horst RJ, Voll LM, Usadel B, Poree F, Stitt M, Pons-Kuhnemann J, Sonnewald U, Kahmann R, et al. 2008. Reprogramming a maize plant: transcriptional and metabolic changes induced by the fungal biotroph *Ustilago maydis*. *Plant Journal* **56**(2): 181-195.

Dutheil JY, Mannhaupt G, Schweizer G, C MKS, Munsterkotter M, Guldener U, Schirawski J, Kahmann R. 2016. A tale of genome compartmentalization: The evolution of virulence clusters in smut fungi. *Genome Biology and Evolution* **8**(3): 681-704.

El Gueddari NE, Rauchhaus U, Moerschbacher BM, Deising HB. 2002. Developmentally regulated conversion of surface‐exposed chitin to chitosan in cell walls of plant pathogenic fungi. *New Phytologist* **156**(1): 103-112.

Flor-Parra I, Castillo-Lluva S, Perez-Martin J. 2007. Polar growth in the infectious hyphae of the phytopathogen ustilago maydis depends on a virulence-specific cyclin. *Plant Cell* **19**(10): 3280-3296.

Fujikawa T, Kuga Y, Yano S, Yoshimi A, Tachiki T, Abe K, Nishimura M. 2009. Dynamics of cell wall components of *Magnaporthe grisea* during infectious structure development. *Molecular Microbiology* **73**(4): 553-570.

Hemetsberger C, Herrberger C, Zechmann B, Hillmer M, Doehlemann G. 2012. The *Ustilago maydis* effector Pep1 suppresses plant immunity by inhibition of host peroxidase activity. *PLoS Pathogens* **8**(5): e1002684.

Hemetsberger C, Mueller AN, Matei A, Herrberger C, Hensel G, Kumlehn J, Mishra B, Sharma R, Thines M, Huckelhoven R, et al. 2015. The fungal core effector Pep1 is conserved across smuts of dicots and monocots. *New Phytologist* **206**(3): 1116-1126.

Huckelhoven R. 2007. Cell wall-associated mechanisms of disease resistance and susceptibility. *Annual Review of Phytopathology* **45**: 101-127.

Kamper J, Kahmann R, Bolker M, Ma LJ, Brefort T, Saville BJ, Banuett F, Kronstad JW, Gold SE, Muller O, et al. 2006. Insights from the genome of the biotrophic fungal plant pathogen *Ustilago maydis*. *Nature* **444**(7115): 97-101.

Kijpornyongpan T, Mondo SJ, Barry K, Sandor L, Lee J, Lipzen A, Pangilinan J, LaButti K, Hainaut M, Henrissat B, et al. 2018. Broad genomic sampling reveals a smut pathogenic ancestry of the fungal clade Ustilaginomycotina. *Molecular Biology and Evolution* **35**(8): 1840-1854.

Kopecka M, Gabriel M. 1992. The influence of congo red on the cell wall and (1----3)-beta-D-glucan microfibril biogenesis in *Saccharomyces cerevisiae*. *Archives of Microbiology* **158**(2): 115-126.

Krombach S, Reissmann S, Kreibich S, Bochen F, Kahmann R. 2018. Virulence function of the *Ustilago maydis* sterol carrier protein 2. *New Phytologist* **220**(2): 553-566.

Kumar S, Stecher G, Tamura K. 2016. MEGA7: Molecular evolutionary genetics analysis version 7.0 for bigger datasets. *Molecular Biology and Evolution* **33**(7): 1870-1874.

Lange J, Mohr U, Wiemken A, Boller T, Vogeli-Lange R. 1996. Proteolytic processing of class IV chitinase in the compatible interaction of bean roots with *Fusarium solani*. *Plant Physiology* **111**(4): 1135-1144.

Lanver D, Muller AN, Happel P, Schweizer G, Haas FB, Franitza M, Pellegrin C, Reissmann S, Altmuller J, Rensing SA, et al. 2018. The biotrophic development of *Ustilago maydis* studied by RNA-Seq analysis. *Plant Cell* **30**(2): 300-323.

Laurie JD, Ali S, Linning R, Mannhaupt G, Wong P, Guldener U, Munsterkotter M, Moore R, Kahmann R, Bakkeren G, et al. 2012. Genome comparison of barley and maize smut fungi reveals targeted loss of RNA silencing components and species-specific presence of transposable elements. *Plant Cell* **24**(5): 1733-1745.

Lo Presti L, Lanver D, Schweizer G, Tanaka S, Liang L, Tollot M, Zuccaro A, Reissmann S, Kahmann R. 2015. Fungal effectors and plant susceptibility. *Annual Review of Plant Biology* **66**: 513-545.

Loubradou G, Brachmann A, Feldbrugge M, Kahmann R. 2001. A homologue of the transcriptional repressor Ssn6p antagonizes cAMP signalling in *Ustilago maydis*. *Molecular Microbiology* **40**(3): 719-730.

Ma LS, Wang L, Trippel C, Mendoza-Mendoza A, Ullmann S, Moretti M, Carsten A, Kahnt J, Reissmann S, Zechmann B, et al. 2018. The *Ustilago maydis* repetitive effector Rsp3 blocks the antifungal activity of mannose-binding maize proteins. *Nature Communications* **9**(1): 1711.

Marshall R, Kombrink A, Motteram J, Loza-Reyes E, Lucas J, Hammond-Kosack KE, Thomma BP, Rudd JJ. 2011. Analysis of two in planta expressed LysM effector homologs from the fungus *Mycosphaerella graminicola* reveals novel functional properties and varying contributions to virulence on wheat. *Plant Physiology* **156**(2): 756-769.

Matei A, Ernst C, Gunl M, Thiele B, Altmuller J, Walbot V, Usadel B, Doehlemann G. 2018. How to make a tumour: cell type specific dissection of *Ustilago maydis*-induced tumour development in maize leaves. *New Phytologist* **217**(4): 1681-1695.

Mendoza-Mendoza A, Berndt P, Djamei A, Weise C, Linne U, Marahiel M, Vranes M, Kamper J, Kahmann R. 2009. Physical-chemical plant-derived signals induce differentiation in *Ustilago maydis*. *Molecular Microbiology* **71**(4): 895-911.

Mentlak TA, Kombrink A, Shinya T, Ryder LS, Otomo I, Saitoh H, Terauchi R, Nishizawa Y, Shibuya N, Thomma BP, et al. 2012. Effector-mediated suppression of chitin-triggered immunity by *Magnaporthe oryzae* is necessary for rice blast disease. *Plant Cell* **24**(1): 322-335.

Mogilnaya OA, Ronzhin NO, Artemenko KS, Bondar VS. 2017. Morphological properties and levels of extracellular peroxidase activity and light emission of the basidiomycete *Armillaria borealis* treated with beta-glucosidase and chitinase. *Mycosphere* **8**(4): 649-659.

Molina L, Kahmann R. 2007. An *Ustilago maydis* gene involved in H_2O_2 detoxification is required for virulence. *Plant Cell* **19**(7): 2293-2309.

Mueller AN, Ziemann S, Treitschke S, Assmann D, Doehlemann G. 2013. Compatibility in the *Ustilago maydis*-maize interaction requires inhibition of host cysteine proteases by the fungal effector Pit2. *PLoS Pathogens* **9**(2): e1003177.

Nampally M, Moerschbacher BM, Kolkenbrock S. 2012. Fusion of a novel genetically engineered chitosan affinity protein and green fluorescent protein for specific detection of chitosan *in vitro* and *in situ*. *Applied and Environmental Microbiology* **78**(9): 3114-3119.

Naumann TA, Wicklow DT, Price NP. 2011. Identification of a chitinase-modifying protein from *Fusarium verticillioides*: truncation of a host resistance protein by a fungalysin metalloprotease. *Journal of Biological Chemistry* **286**(41): 35358-35366.

Okmen B, Kemmerich B, Hilbig D, Wemhoner R, Aschenbroich J, Perrar A, Huesgen PF, Schipper K, Doehlemann G. 2018. Dual function of a secreted fungalysin metalloprotease in *Ustilago maydis*. *New Phytologist* **220**(1): 249-261.

Rabe F, Bosch J, Stirnberg A, Guse T, Bauer L, Seitner D, Rabanal FA, Czedik-Eysenberg A, Uhse S, Bindics J, et al. 2016. A complete toolset for the study of *Ustilago bromivora* and *Brachypodium* sp. as a fungal-temperate grass pathosystem. *eLife* **5**: e20522.

Ram AF, Klis FM. 2006. Identification of fungal cell wall mutants using susceptibility assays based on Calcofluor white and Congo red. *Nature Protocols* **1**(5): 2253-2256.

Rooney HC, Van't Klooster JW, van der Hoorn RA, Joosten MH, Jones JD, de Wit PJ. 2005. Cladosporium Avr2 inhibits tomato Rcr3 protease required for *Cf-2*-dependent disease resistance. *Science* **308**(5729): 1783-1786.

Ruiz-Herrera J, Ortiz-Castellanos L, Martinez AI, Leon-Ramirez C, Sentandreu R. 2008. Analysis of the proteins involved in the structure and synthesis of the cell wall of *Ustilago maydis*. *Fungal Genetics and Biology* **45 Suppl 1**: S71-76.

Sanchez-Vallet A, Saleem-Batcha R, Kombrink A, Hansen G, Valkenburg DJ, Thomma BP, Mesters JR. 2013. Fungal effector Ecp6 outcompetes host immune receptor for chitin binding through intrachain LysM dimerization. *eLife* **2**: e00790.

Schirawski J, Mannhaupt G, Munch K, Brefort T, Schipper K, Doehlemann G, Di Stasio M, Rossel N, Mendoza-Mendoza A, Pester D, et al. 2010. Pathogenicity determinants in smut fungi revealed by genome comparison. *Science* **330**(6010): 1546-1548.

Schuster M, Schweizer G, Kahmann R. 2018. Comparative analyses of secreted proteins in plant pathogenic smut fungi and related basidiomycetes. *Fungal Genetics and Biology* **112**: 21-30.

Seitner D, Uhse S, Gallei M, Djamei A. 2018. The core effector Cce1 is required for early infection of maize by *Ustilago maydis*. *Molecular Plant Pathology* **19**(10): 2277-2287.

Sharma R, Mishra B, Runge F, Thines M. 2014. Gene loss rather than gene gain is associated with a host jump from monocots to dicots in the smut fungus *Melanopsichium pennsylvanicum*. *Genome Biology and Evolution* **6**(8): 2034-2049.

Song J, Win J, Tian M, Schornack S, Kaschani F, Ilyas M, van der Hoorn RA, Kamoun S. 2009. Apoplastic effectors secreted by two unrelated eukaryotic plant pathogens target the tomato defense protease Rcr3. *Proceedings of the National Academy of Sciences, USA* **106**(5): 1654-1659.

Takahara H, Hacquard S, Kombrink A, Hughes HB, Halder V, Robin GP, Hiruma K, Neumann U, Shinya T, Kombrink E, et al. 2016. *Colletotrichum higginsianum* extracellular LysM proteins play dual roles in appressorial function and suppression of chitin-triggered plant immunity. *New Phytologist* **211**(4): 1323-1337.

Tanaka S, Brefort T, Neidig N, Djamei A, Kahnt J, Vermerris W, Koenig S, Feussner K, Feussner I, Kahmann R. 2014. A secreted *Ustilago maydis* effector promotes virulence by targeting anthocyanin biosynthesis in maize. *eLife* **3**: e01355.

Tanaka S, Djamei A, Presti LL, Schipper K, Winterberg S, Amati S, Becker D, Buchner H, Kumlehn J, Reissmann S, et al. 2015a. Experimental approaches to investigate effector translocation into host cells in the *Ustilago maydis*/maize pathosystem. *European Journal of Cell Biology* **94**(7-9): 349-358.

Tanaka S, Han X, Kahmann R. 2015b. Microbial effectors target multiple steps in the salicylic acid production and signaling pathway. *Frontiers in Plant Science* **6**: 349.

Tanaka S, Schweizer G, Rossel N, Fukada F, Thines M, Kahmann R. 2019. Neofunctionalization of the secreted Tin2 effector in the fungal pathogen *Ustilago maydis*. *Nature Microbiology* **4**(2): 251-257.

Tian M, Benedetti B, Kamoun S. 2005. A Second Kazal-like protease inhibitor from *Phytophthora infestans* inhibits and interacts with the apoplastic pathogenesis-related protease P69B of tomato. *Plant Physiology* **138**(3): 1785-1793.

Tian M, Huitema E, Da Cunha L, Torto-Alalibo T, Kamoun S. 2004. A Kazal-like extracellular serine protease inhibitor from *Phytophthora infestans* targets the tomato pathogenesis-related protease P69B. *Journal of Biological Chemistry* **279**(25): 26370-26377.

Tian M, Win J, Song J, van der Hoorn R, van der Knaap E, Kamoun S. 2007. A *Phytophthora infestans* cystatin-like protein targets a novel tomato papain-like apoplastic protease. *Plant Physiology* **143**(1): 364-377.

Toruno TY, Stergiopoulos I, Coaker G. 2016. Plant-pathogen effectors: cellular probes interfering with plant defenses in spatial and temporal manners. *Annual Review of Phytopathology* **54**: 419-441.

Underwood W. 2012. The plant cell wall: a dynamic barrier against pathogen invasion. *Frontiers in Plant Science* **3**: 85.

van den Burg HA, Harrison SJ, Joosten MH, Vervoort J, de Wit PJ. 2006. *Cladosporium fulvum* Avr4 protects fungal cell walls against hydrolysis by plant chitinases accumulating during infection. *Molecular Plant-Microbe Interactions* **19**(12): 1420-1430.

van Esse HP, Van't Klooster JW, Bolton MD, Yadeta KA, van Baarlen P, Boeren S, Vervoort J, de Wit PJ, Thomma BP. 2008. The *Cladosporium fulvum* virulence protein Avr2 inhibits host proteases required for basal defense. *Plant Cell* **20**(7): 1948-1963.

Vanky K, Lutz M, Bauer R. 2008. About the genus *Thecaphora* (Glomosporiaceae) and its new synonyms. *Mycological Progress* **7**: 31-39.

Villajuana-Bonequi M, Matei A, Ernst C, Hallab A, Usadel B, Doehlemann G. 2019. Cell type specific transcriptional reprogramming of maize leaves during *Ustilago maydis* induced tumor formation. *Scientific Reports* **9**(1): 10227.

Vollmeister E, Schipper K, Baumann S, Haag C, Pohlmann T, Stock J, Feldbrugge M. 2012. Fungal development of the plant pathogen *Ustilago maydis*. *FEMS Microbiology Reviews* **36**(1): 59-77.

Wang Y, Wang Y. 2018. Trick or treat: microbial pathogens evolved apoplastic effectors modulating plant susceptibility to infection. *Molecular Plant-Microbe Interactions* **31**(1): 6-12.

Wedlich-Soldner R, Bolker M, Kahmann R, Steinberg G. 2000. A putative endosomal t-SNARE links exo- and endocytosis in the phytopathogenic fungus *Ustilago maydis*. *EMBO Journal* **19**(9): 1974-1986.

Wosten HA, Bohlmann R, Eckerskorn C, Lottspeich F, Bolker M, Kahmann R. 1996. A novel class of small amphipathic peptides affect aerial hyphal growth and surface hydrophobicity in *Ustilago maydis*. *EMBO Journal* **15**(16): 4274-4281.

Ye Z, Pan Y, Zhang Y, Cui H, Jin G, McHardy AC, Fan L, Yu X. 2017. Comparative whole-genome analysis reveals artificial selection effects on *Ustilago esculenta* genome. *DNA Research* **24**(6): 635-648.

Zambanini T, Buescher JM, Meurer G, Wierckx N, Blank LM. 2016. Draft genome sequence of *Ustilago trichophora* RK089, a promising malic acid producer. *Genome Announcements* **4**(4): e00749-00716.

Zuo W, Okmen B, Depotter JRL, Ebert MK, Redkar A, Misas Villamil J, Doehlemann G. 2019. Molecular interactions between smut fungi and their host plants. *Annual Review of Phytopathology* **57**: 411-430.

The following Supporting Information is available for this article:

Fig. S1. Virulence of deletion mutants of *sta1* in haploid strains.

Fig. S2. Fungal colonization of SG200 and SG200Δsta1 in maize leaf tissue.

Fig. S3. Comparison of autofluorescence in the leaf tissues infected with SG200 and SG200Δsta1.

Fig. S4. qRT-PCR analysis of genes from the phenylpropanoid pathway after infection with SG200 and SG200Δsta1.

Fig. S5. Amino acid alignment of Sta1 orthologs.

Fig. S6. Plasmolysis assay of the leaf tissues infected with strain expressing Sta1-mCherry-HA.

Fig. S7. Immunostaining of Sta1-3xHA protein in filament on parafilm.

Fig. S8. Immunostaining of Sta1-3xHA protein in budding cells on parafilm.

Fig. S9. Immunostaining of Sta1-3xHA protein in budding cells on PD plate.

Fig. S10. Hydrophobicity of filamentous colonies of SG200 and SG200Δsta1:P_{actin}-Sta1-3xHA.

Fig. S11. Stress assay of SG200Δsta1:P_{actin}-Sta1-3xHA on PD-Congo red plate.

Fig. S12. Microscopic picture of filamentous cells treated with β-glucanase.

Fig. S13. β-glucanase and chitinase treatment of budding cells constitutively expressing Sta1-3xHA.

Fig. S14. Filamentous colonies and stress assays of *sta1* mutant.

Fig. S15. Pathogenicity assay of SG200Δsta1:P_{actin}-Sta1-3xHA.

Table S1. Raw data for infection assays.

Table S2. Plasmids used in this study.

Table S3. Primers used in this study.

Table S4. *U. maydis* strains used in this study.

Table S5. Amino acid identity between Sta1 orthologs.

Figure legends

Fig. 1. Identification of Sta1 as a novel effector required for virulence in *Ustilago maydis*. (a) The expression pattern of *U. maydis sta1* (*UMAG_12226*) gene during plant infection retrieved from RNA-seq data (Lanver *et al.*, 2018). A.C. indicates the expression level in axenic culture. The number below the bar indicates the day post inoculation (dpi). Error bars indicate ± standard deviations. (b) Schematic picture of *U. maydis* Sta1 protein structure. The protein comprises 169 amino acids with N-terminal secretion signal (1-23 aa). The numbers indicate the position of cysteine residues. (c) Macroscopic picture of maize leaves infected by *U. maydis* SG200Δsta1 mutants at 12 dpi. (d) Pathogenicity assay of the *sta1* mutant and complementation strains in *U. maydis*. Disease symptoms were quantified based on three biological replicates. The mean percentage of plants placed in a certain disease category is indicated. The number of infected plants is indicated at the top of the bar. The asterisk indicates significant differences of disease symptoms in SG200Δsta1 compared to SG200 determined by a two-tailed Student's *t*-test ($p<0.05$).

Fig. 2. Fungal colonization and development of tumor tissues in leaf tissues infected with *Ustilago maydis* strains. (a) Three-dimensional confocal microscopy of leaf tissue infected with *U. maydis* SG200 and SG200Δsta1 at 2 dpi (left). Green color indicates fungal hyphae. Red color indicates vascular bundles. Bar = 50 μm. A schematic of fungal infection is shown (right). (b) Microscopic picture of leaf cross section inoculated with H_2O (mock), *U. maydis* SG200 and SG200Δsta1 at 6 dpi. Plant cell walls are visualized by autofluorescence (blue). Fungal hyphae are stained by WGA-AF488 (yellow). White color indicates overlap of the signal from autofluorescence and WGA-AF488. Vascular bundles (Vb) are highlighted by dotted white line. Bar = 100 μm.

Fig. 3. Sta1 orthologs are functionally conserved in the related smut pathogens. (a) Schematic picture of gene locus encoding *sta1* ortholog of *Ustilago maydis* in the related smut pathogens from *Sporisorium reilianum* f.sp. *zeae*, *Ustilago hordei*, *Melanopsichium pennsylvanicum*, *Testicularia cyperi* and *Thecaphora thlaspeos*. (b) Phylogenetic relationship of plant pathogenic smut fungi. The rDNA ITS sequences from *U. maydis*, *U. hordei*, *S. reilianum*, *S. scitamineum*, *M. pennsylvanicum*

(Ustilaginaceae), *T. cyperi* (Anthracoideaceae), *T. thlaspeos* (Glomosporiaceae), *Malassezia globosa* and *Phytophthora infestans* were aligned by Clustal Omega. The phylogenetic tree was constructed using MEGA 7.0 software (Kumar *et al.*, 2016) using the Maximum Likelihood method with Tamura-Nei model, 1000 bootstrap replicates and complete gap deletion. The bootstrap values are indicated on each branch. *P. infestans* was used as outgroup. (c) Pathogenicity assay of *U. maydis sta1* mutants complemented with respective orthologs from Ustilaginaceae. Disease symptoms were quantified based on three biological replicates. The mean percentage of plants placed in a certain disease category is indicated. The number of infected plants is indicated at the top of the bar. The asterisks indicate significant differences of disease symptoms in respective complementation strains compared to SG200Δsta1 determined by a two-tailed Student's *t*-test ($p<0.05$). (d) Pathogenicity assay of *U. maydis sta1* mutants complemented with an ortholog from *T. cyperi*. Disease symptoms were quantified based on three biological replicates. The mean percentage of plants placed in a certain disease category is indicated. The number of infected plants is indicated at the top of the bar. The asterisks indicate significant differences of disease symptoms in individual complementation strains compared to SG200Δsta1 determined by a two-tailed Student's *t*-test ($p<0.05$).

Fig. 4. Sta1 is a secreted protein. (a) Confocal microscopy of *Ustilago maydis* strains expressing Sta1-mCherry-HA or mCherry-HA in leaf epidermal cells at 2 d post inoculation (dpi). Bar = 10 μm. (b) Immunoprecipitation of Sta1-3xHA protein from axenic culture supernatant of *U. maydis* SG200Δsta1:P_{actin}-Sta1-3xHA that constitutively expresses Sta-3xHA. (c) Immunoprecipitation of mCherry-HA protein carrying signal peptide (SP) at N-terminus and Sta1-HA protein. Maize leaf tissue was infected with the *U. maydis* strains expressing respective proteins. Total protein was extracted with buffer lacking SDS. (d) Immunoprecipitation of Sta1-HA protein. Maize leaf tissue was infected with the *U. maydis* strains expressing respective proteins. Total protein was extracted with buffer containing 0.1% SDS. Asterisks indicate full-length protein.

Fig. 5. Sta1 is attached to the surface of fungal filaments of *Ustilago maydis*. (a) Immunostaining of Sta1-3xHA protein in budding cells from *U. maydis* SG200 and SG200Δsta1:P_{actin}-Sta1-3xHA. Bar = 25 μm. (b) Immunostaining of Sta1-3xHA protein in filamentous cells from *U. maydis* SG200 and

SG200Δsta1:P_{actin}-Sta1-3xHA on parafilm. Green signal of Alexa Fluor 488 (AF488) indicates the localization of Sta1-3xHA. Bar = 25 μm.

Fig. 6. Visualization of Sta1-3xHA protein and fungal plasma membrane in filament of *Ustilago maydis*. (a) Immunostaining of filament of *U. maydis* SG200Δsta1:P_{actin}-Sta1-3xHA. Localization of Sta1-3xHA was visualized by Alexa Fluor 488 (AF488; green) and fungal plasma membrane was visualized by FM4-64 (red). Bar = 1 μm. (b) Plasmolysis in filament of *U. maydis* SG200Δsta1:P_{actin}-Sta1-3xHA. Localization of Sta1-3xHA was visualized by Alexa Fluor 488 (AF488; green) and fungal plasma membrane was visualized by FM4-64 (red). Plasmolysis (which took about 1 hour) was indicated by arrow. Bar = 3 μm.

Fig. 7. Sta1 expression alters the property of fungal filaments of *Ustilago maydis*. (a) Microscopic picture of the edge of a filamentous colony of *U. maydis* SG200, SG200Δsta1:P_{actin}-Sta1-3xHA and SG200Δsta1:P_{actin}-Tin2-3xHA on PD-charcoal plate. Bar = 500 μm. (b) Multiple stress assay for filamentation of *U. maydis* SG200, SG200Δsta1:P_{actin}-Sta1-3xHA and SG200Δsta1:P_{actin}-Tin2-3xHA on PD-charcoal plates containing Congo red, Calcofluor white, H_2O_2 and SDS. (c) Macroscopic picture of filamentous colony of *U. maydis* SG200, SG200Δsta1:P_{actin}-Sta1-3xHA and SG200Δsta1:P_{actin}-Tin2-3xHA on PD-charcoal plates after dropping β-glucanase or chitinase. Bar = 1 mm. (d) Microscopic picture of filamentous cells of *U. maydis* SG200 and SG200Δsta1:P_{actin}-Sta1-3xHA after treatment by chitinase *in vitro*. Bar = 35 μm.

Fig. 8. Altered timing of *sta1* expression interferes with the virulence function of Sta1 in *Ustilago maydis*. (a) The expression pattern of *U. maydis UMAG_04033* gene during plant infection retrieved from RNA-seq data (Lanver *et al.*, 2018). A.C. indicates the expression level in axenic culture. The number below the bar indicates the day post inoculation (dpi). Error bars indicate standard deviations. (b) Pathogenicity assay of *U. maydis sta1* mutants complemented with *sta1* expressed under *UMAG_04033* promoter. Disease symptoms were quantified based on three biological replicates. The mean percentage of plants placed in a certain disease category is indicated. The number of infected plants is indicated at the top of the bar. The asterisks indicate significant differences of disease symptoms in SG200Δsta1:P_{UMAG_04033}-Sta1 compared to SG200 determined by a two-tailed Student's *t*-test ($p<0.05$).

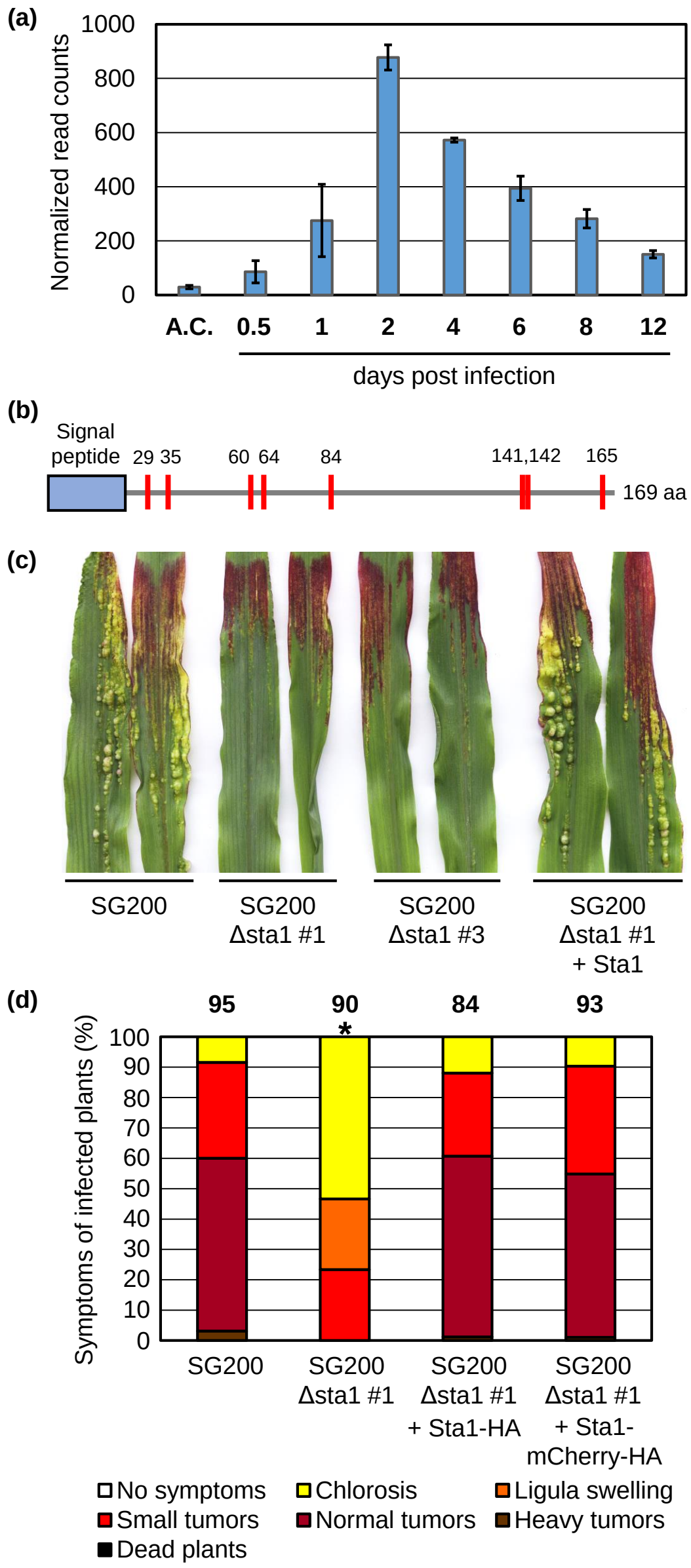
(a)
Normalized read counts
1000
800
600
400
200
0
A.C.
0.5
1
2
4
6
8
12
days post infection
(b)
Signal peptide
29 35
60 64
84
141,142
165
169 aa
(c)
SG200
SG200 Δsta1 #1
SG200 Δsta1 #3
SG200 Δsta1 #1 + Sta1
(d)
95
90
*
84
93
Symptoms of infected plants (%)
100
90
80
70
60
50
40
30
20
10
0
SG200
SG200 Δsta1 #1
SG200 Δsta1 #1 + Sta1-HA
SG200 Δsta1 #1 + Sta1-mCherry-HA
No symptoms
Chlorosis
Ligula swelling
Small tumors
Normal tumors
Heavy tumors
Dead plants

Fig.1.

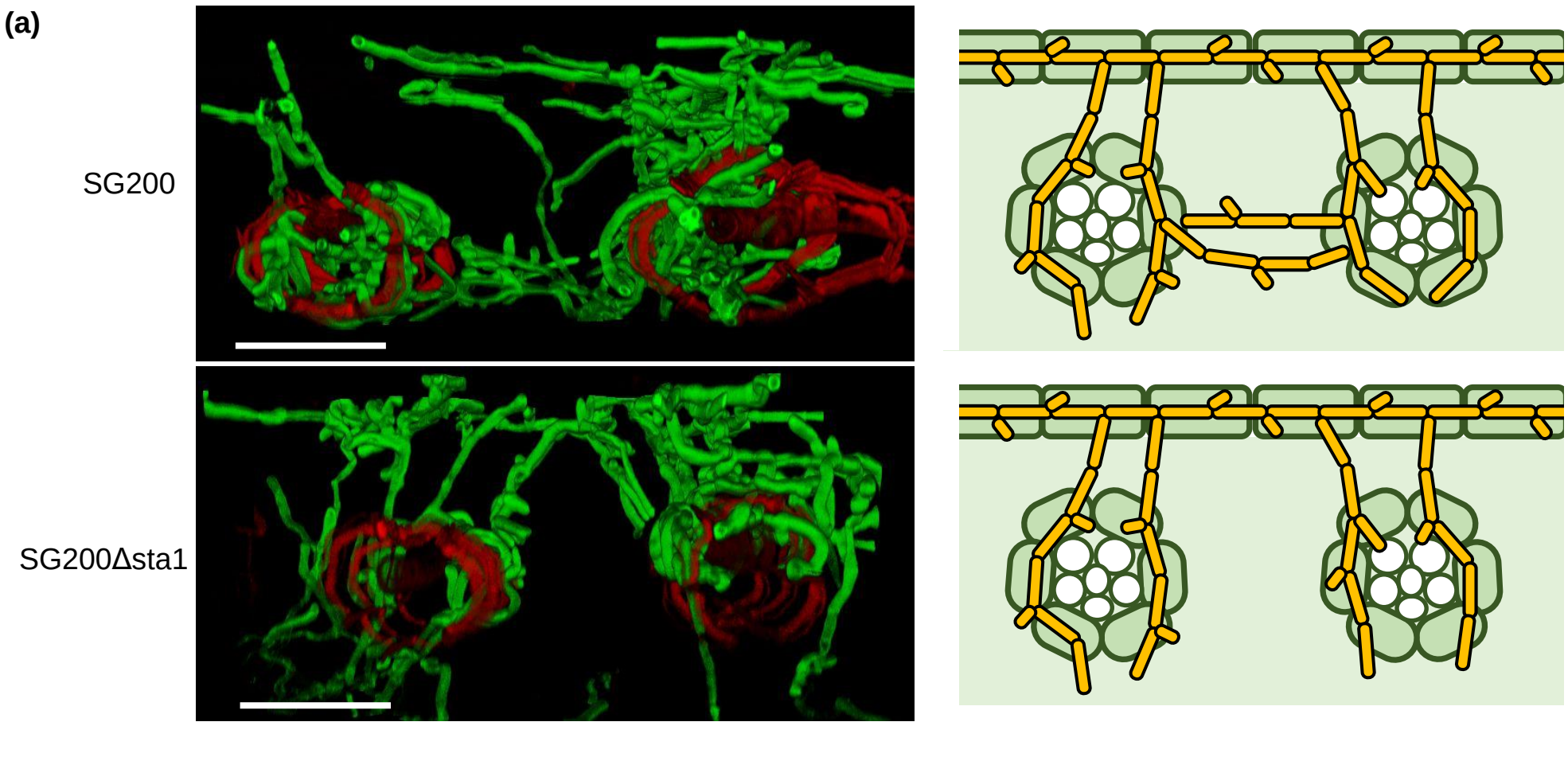

Fig. 2.

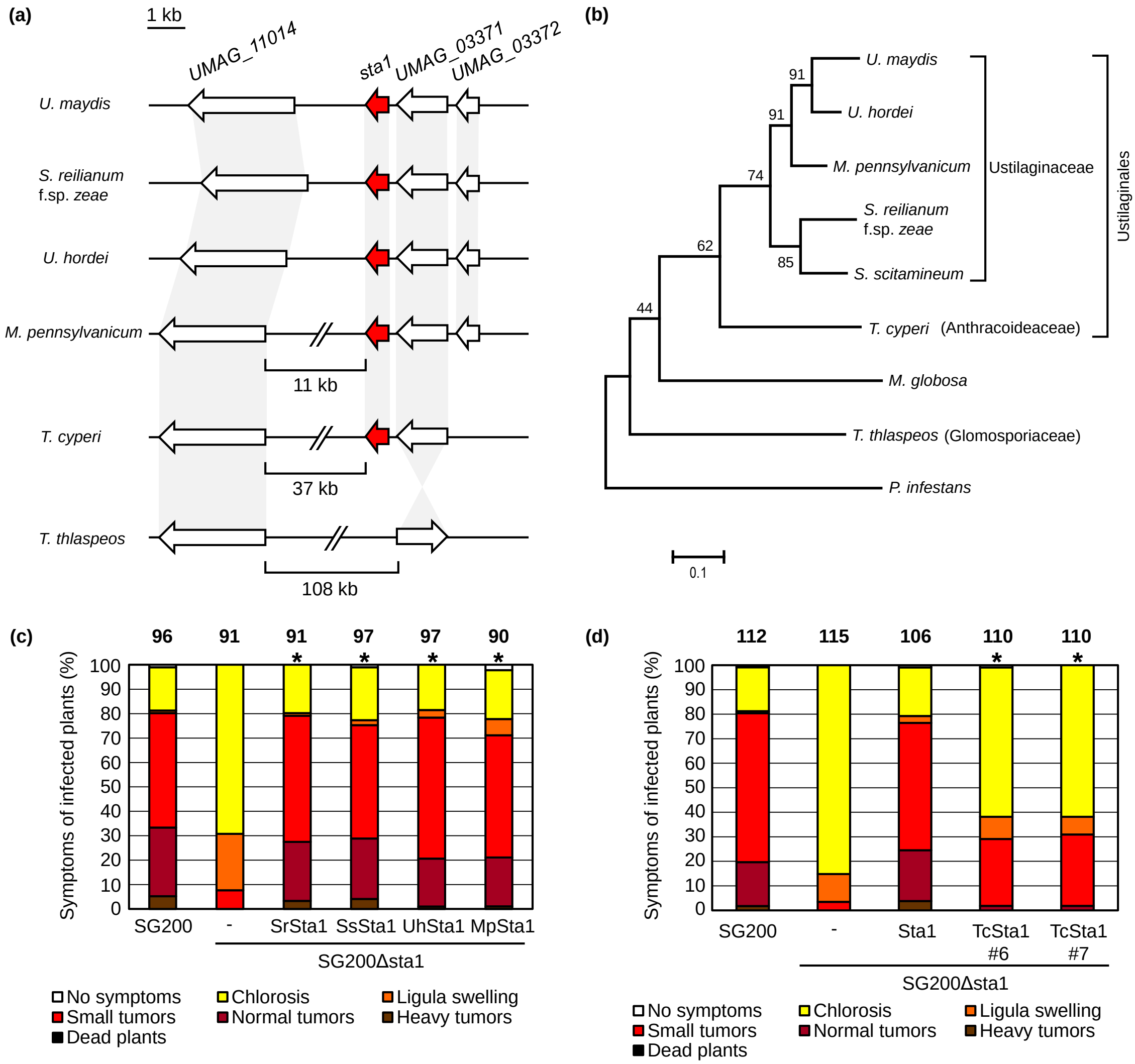
(a)
1 kb
UMAG_11014
sta1
UMAG_03371
UMAG_03372
U. maydis
S. reilianum f.sp. zeae
U. hordei
M. pennsylvanicum
11 kb
T. cyperi
37 kb
T. thlaspeos
108 kb
(b)
U. maydis
U. hordei
M. pennsylvanicum
S. reilianum f.sp. zeae
S. scitamineum
Ustilaginaceae
Ustilaginales
T. cyperi (Anthracoideaceae)
M. globosa
T. thlaspeos (Glomosporiaceae)
P. infestans
91
91
74
62
85
44
0.1
(c)
96
91
91
97
97
90
Symptoms of infected plants (%)
SG200
-
SrSta1
SsSta1
UhSta1
MpSta1
SG200Δsta1
No symptoms
Chlorosis
Ligula swelling
Small tumors
Normal tumors
Heavy tumors
Dead plants
(d)
112
115
106
110
110
Symptoms of infected plants (%)
SG200
-
Sta1
TcSta1 #6
TcSta1 #7
SG200Δsta1
No symptoms
Chlorosis
Ligula swelling
Small tumors
Normal tumors
Heavy tumors
Dead plants

Fig. 3.

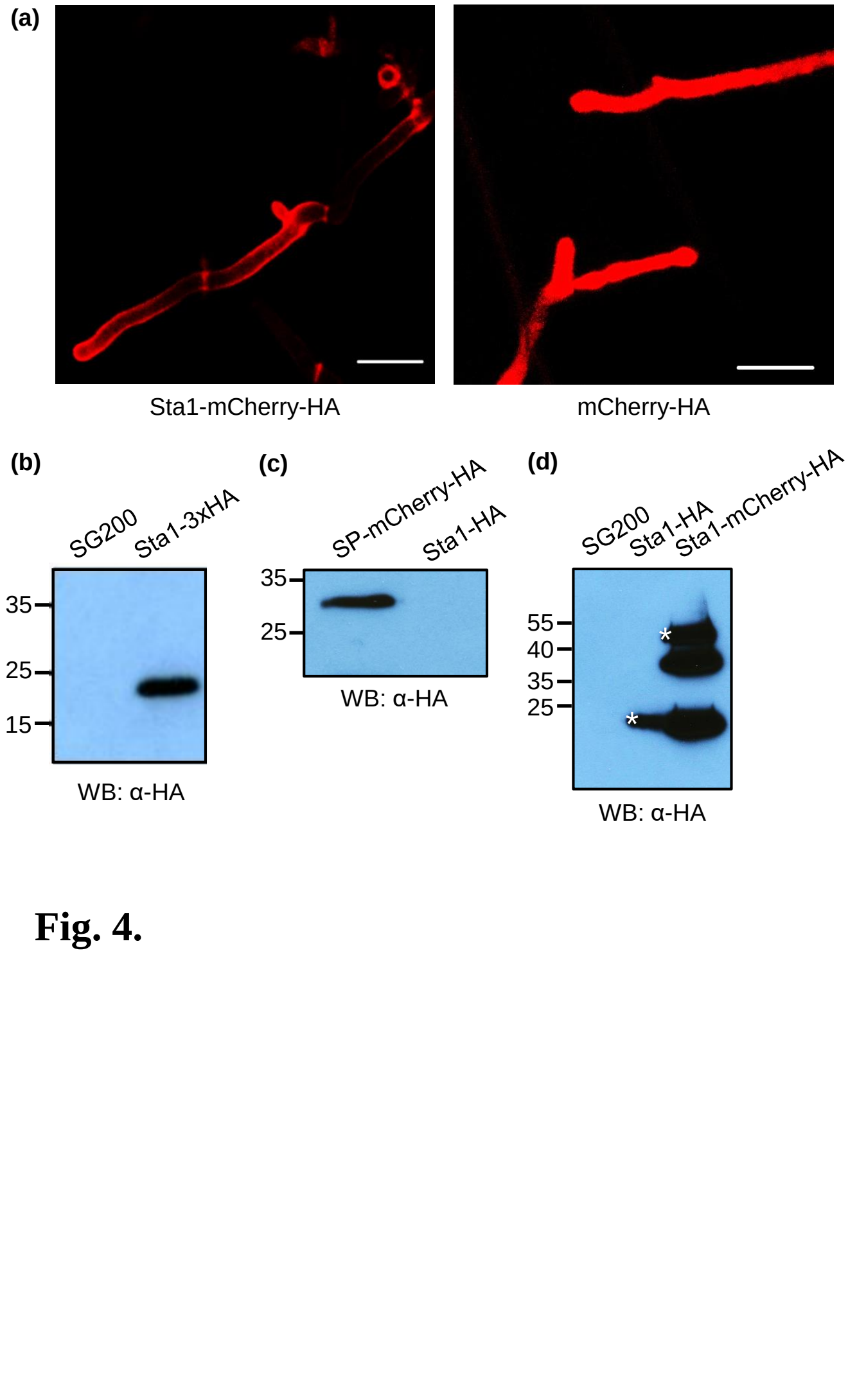
(a)
Sta1-mCherry-HA
mCherry-HA
(b)
SG200
Sta1-3xHA
35
25
15
WB: α-HA
(c)
SP-mCherry-HA
Sta1-HA
35
25
WB: α-HA
(d)
SG200
Sta1-HA
Sta1-mCherry-HA
55
40
35
25
*
*
WB: α-HA

Fig. 4.

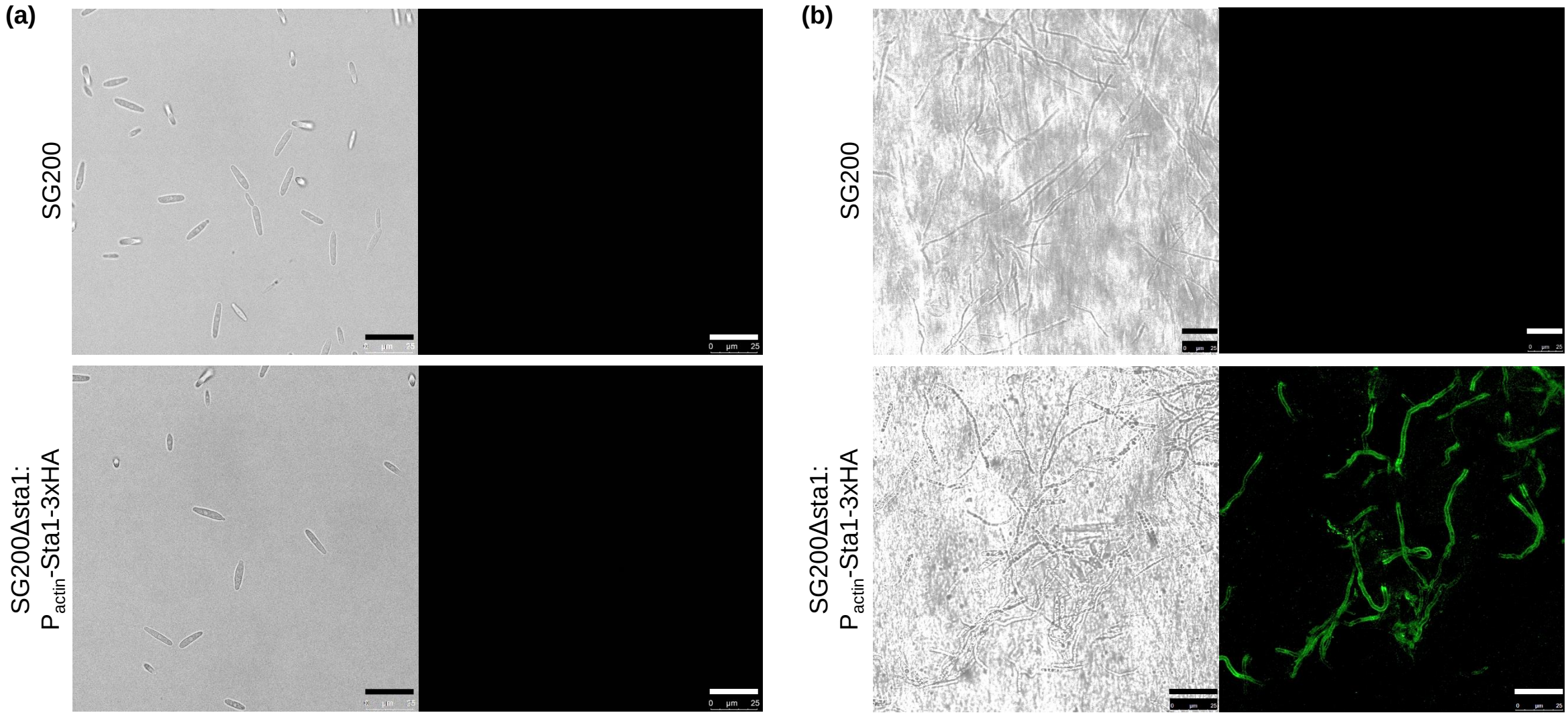
(a)
(b)
SG200
SG200Δsta1:
P$_{actin}$-Sta1-3xHA
Bright field
AF488
Bright field
AF488

Fig. 5.

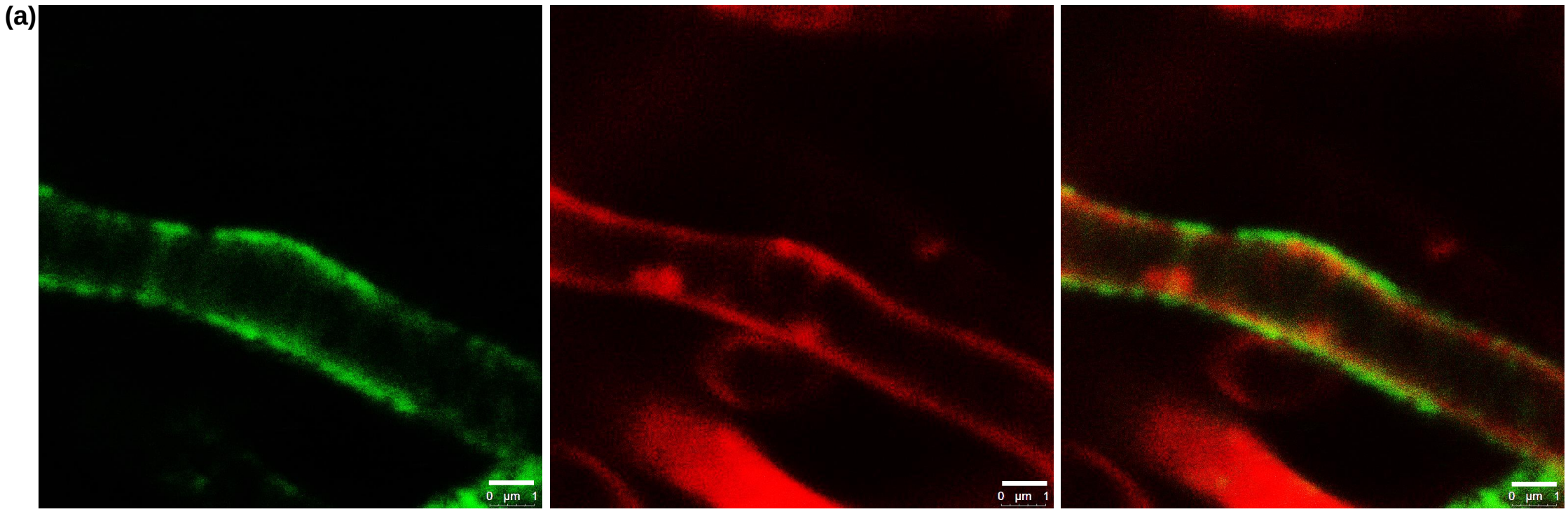
(a)
0 µm 1
0 µm 1
0 µm 1
AF488
FM4-64
Merge
(b)
0 µm 3
0 µm 3
0 µm 3
AF488
FM4-64
Merge

Fig. 6.

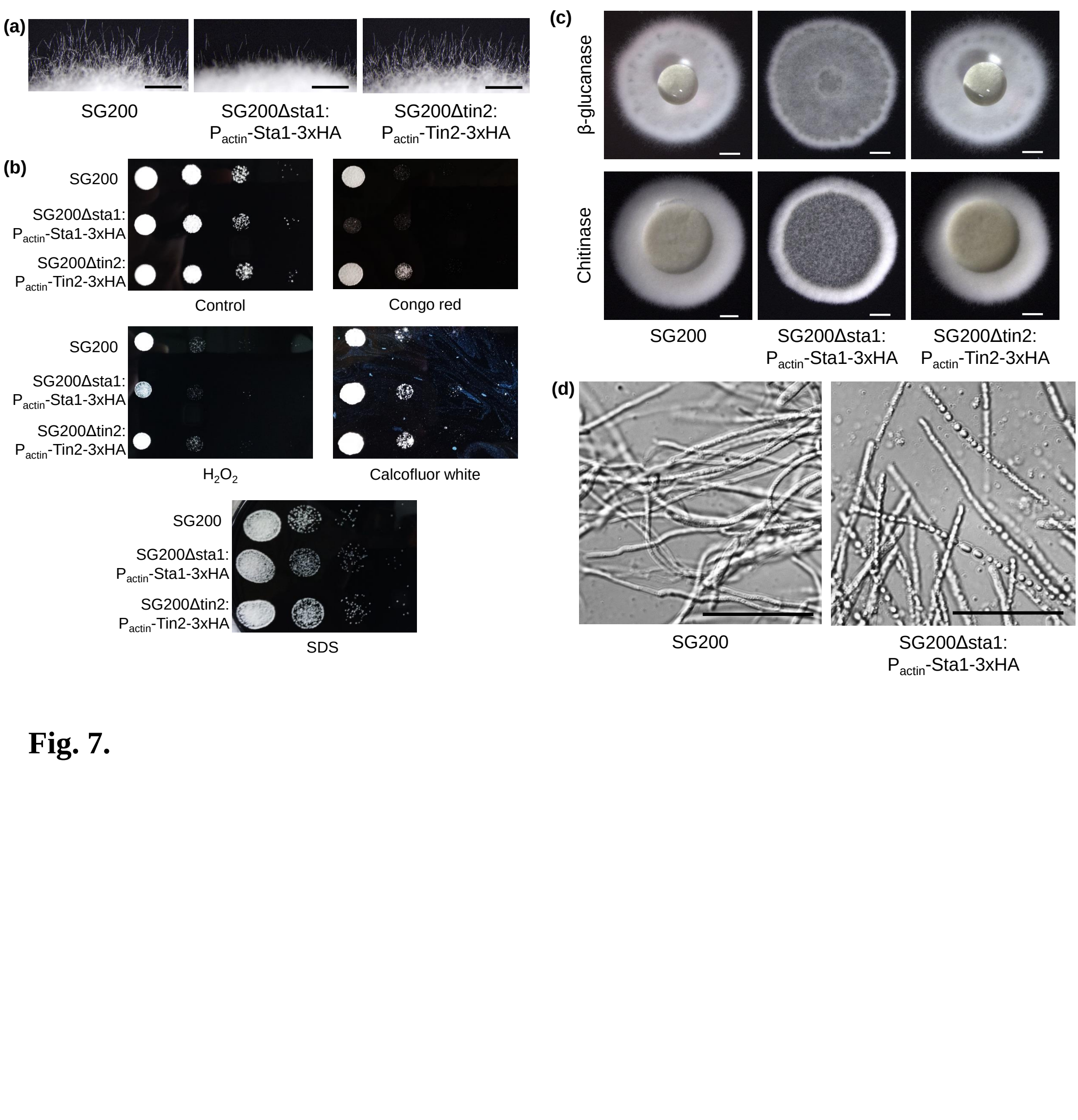
(a)
SG200
SG200Δsta1: Pactin-Sta1-3xHA
SG200Δtin2: Pactin-Tin2-3xHA
(b)
SG200
SG200Δsta1: Pactin-Sta1-3xHA
SG200Δtin2: Pactin-Tin2-3xHA
Control
Congo red
H2O2
Calcofluor white
SDS
(c)
β-glucanase
Chitinase
SG200
SG200Δsta1: Pactin-Sta1-3xHA
SG200Δtin2: Pactin-Tin2-3xHA
(d)
SG200
SG200Δsta1: Pactin-Sta1-3xHA

Fig. 7.

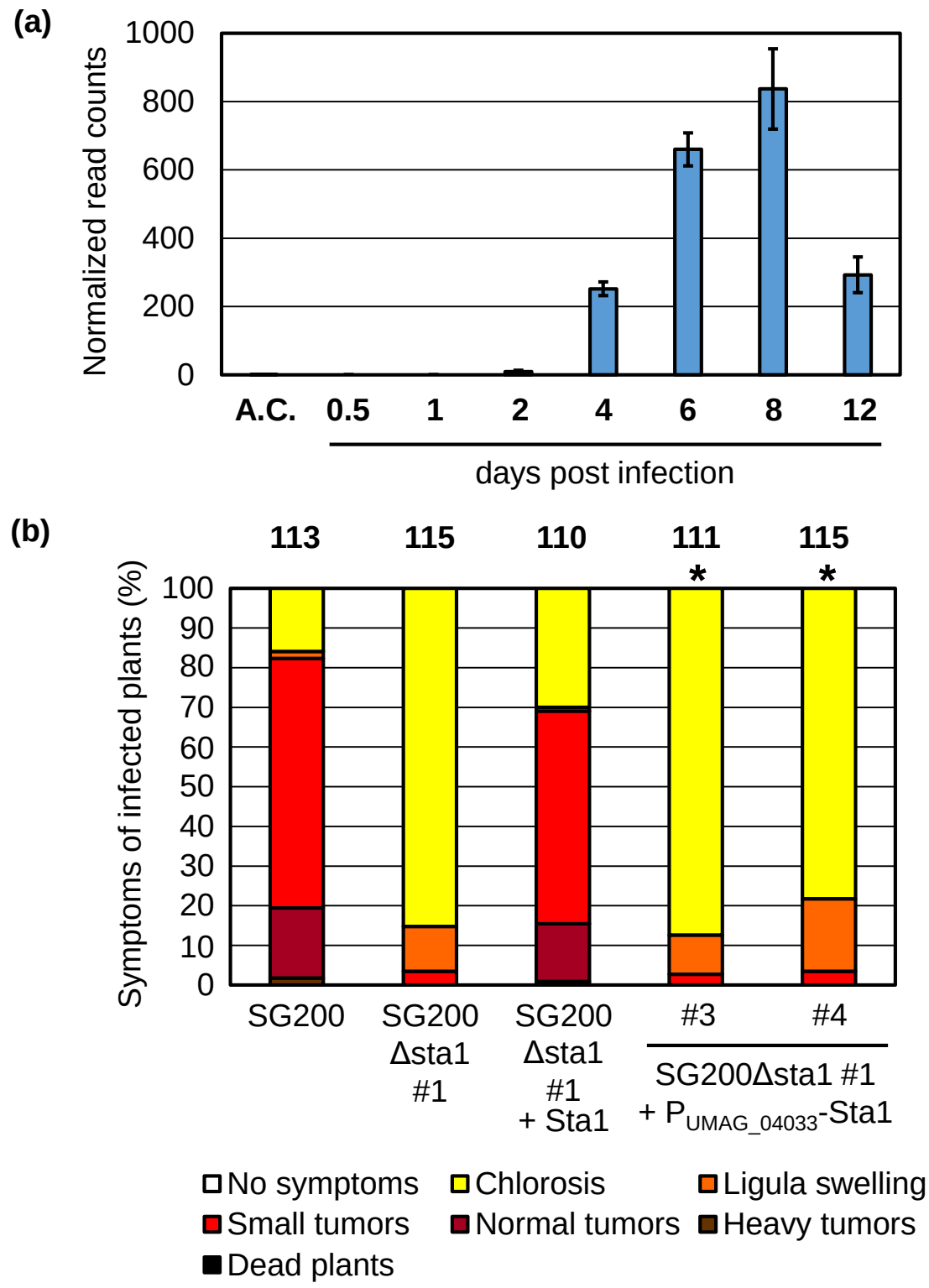
(a)
Normalized read counts
1000
800
600
400
200
0
A.C.
0.5
1
2
4
6
8
12
days post infection
(b)
Symptoms of infected plants (%)
100
90
80
70
60
50
40
30
20
10
0
113
115
110
111
115
*
*
SG200 Δsta1 #1
SG200 Δsta1 #1 + Sta1
SG200Δsta1 #1 + P UMAG_04033 -Sta1
#3
#4
No symptoms
Chlorosis
Ligula swelling
Small tumors
Normal tumors
Heavy tumors
Dead plants

Fig. 8.